SESSION 2

Analysis and Experiment

SIMULATION OF AIR CUSHION HEAVE DYNAMICS WITH VENT VALVE RELAY CONTROL

J.R. Amyot

National Research Council of Canada
Ottawa, Canada

ABSTRACT

A hybrid computer model of the heave dynamics of an air cushion with a segmented skirt and an automatic vent valve control system was used to investigate the effects of relay control threshold velocity on dynamic performance and make comparisons with proportional control. Results have shown that relay control can work well under certain conditions but proportional control is generally better.

INTRODUCTION

Previous computer studies[1,2] have predicted improved heave dynamics damping of nominally-underdamped, but stable, air cushion vehicles (ACVs) with automatic vent valve control wherein valve displacement was made proportional to heave velocity of the platform. Almost equally-good results were obtained regardless of whether the vent valve's set point position was fully-closed or partially-open. Therefore, the fully-closed set point position was considered preferable in order to minimize fuel consumption.

Using the same air cushion system model, this paper presents further proportional control results pertaining to operation at destabilizing values of airflow. However, its main objective is the performance of relay (also called 'on-off' or 'bang-bang') control systems since they tend to be simpler to implement in practice. The same model with a suitably-modified control system was used for this purpose.

CONCEPTUAL MODEL

The system studied is conceptualized in the overview information flow diagram of Fig. 1 which can be subdivided into two subsystems: (1) air cushion heave dynamics which depend on such cushion parameters as bearing area and cushion volume, and (2) the vent valve control system which includes a high pass filter, control algorithm, and actuator and valve dynamics. The first-order high pass filter (Fig. 2) makes the control system less sensitive to low operating frequencies below break frequency ω_a than to high transient frequencies above ω_a, thereby allowing unwanted high frequency components of velocity to

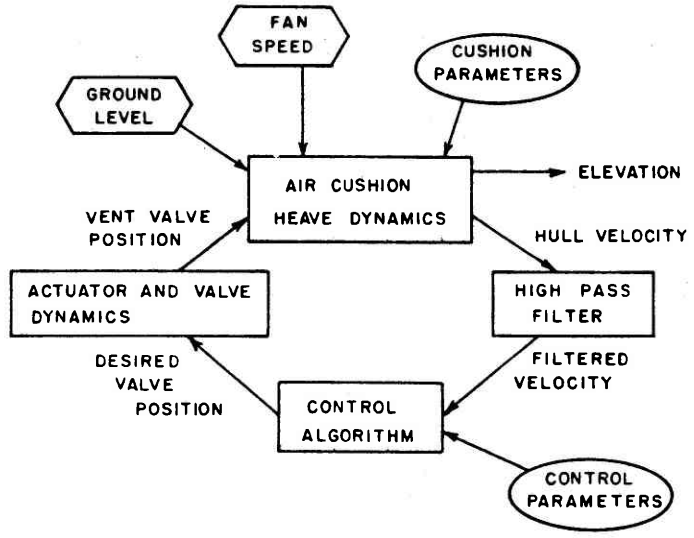


Fig. 1: System overview information flow diagram

be attenuated by the control system while permitting normal operation of the vehicle. The control system's performance depends especially on the control algorithm and its parameters. In the case of proportional control, the desired valve position is proportional to the filtered velocity by a factor K_p. Also shown in Fig. 1 are fan speed and ground level inputs. The former is under manual control in normal ACV operation whereas ground level variations are disturbances whose effects on heave motion are to be minimized. Here, downward steps in ground level were used for test purposes.

The detailed mathematical description of the air cushion heave dynamics and proportional control system used in this study appears in references 1 and 2. The control algorithm was modified for relay control according to the information flow diagram of Fig. 2. In this case, the vent valves move from a closed to fully-open position as rapidly as the actuator and valve dynamcis will allow whenever the hull's filtered velocity $\dot{Z}_f$ exceeds an adjustable threshold velocity ϵ_o. Physically, when the hull reaches a low point in heave motion and starts to rise again with a positive velocity exceeding ϵ_o, the vent valves are opened to reduce the upward propelling force. When it approaches a high point with its velocity decreasing to less than ϵ_o, the vent valves are closed to establish a cushion pressure which will tend to prevent the falling hull from hitting the ground.

SIMULATION RESULTS

The conceptual model was implemented on a hybrid computer to obtain an interactive synchronous model operated at one-twentieth of real time as described in reference 1 and 2. The results obtained from simulation runs are discussed under the following three headings.

Limit Cycle

Trajectories A, B and C in the phase plane $(Z', \dot{Z})$ of Fig. 3 were obtained by operating the system at a steady hover elevation Z_o = 12 cm and applying downward ground steps of 1 cm, 2 cm and 9.5 cm, respectively. Only a finite time portion of the trajectories are shown to avoid cluttering the figure unnecessarily. A complete presentation would show trajectory A eventually converging to (0,0) with increasing time, B diverging to the stable limit cycle (SLC), and C converging to the SLC. Somewhere between trajectories A and B, there exists an unstable limit cycle (ULC), which defines the stable region of the system in the phase plane. Thus, if a trajectory were to begin on the ULC, it could not remain on it. Depending on disturbances, however small, the trajectory would depart from the ULC and either converge to (0,0) with time or diverge to the SLC.

Fan speed is a dominant factor determining the existence and size of limit cycles. The stable region tends to diminish and the size of the SLC tends to increase with increase in fan speed. When the stable region is negligibly small, the system is 'unconditionally unstable'. Conversely, when it encompasses the entire practical region of the phase plane, the sytem is 'stable'. Between these two extremes, it is 'marginally unstable'. Within a stable region, the system may be 'underdamped' or 'well-damped' depending respectively on whether the number of encirclements of the origin is large or small.

Underdamped Stable System

Figure 4 presents velocity attenuation and valve activity as functions of threshold velocity for a downward step in ground level applied to a nominally underdamped stable system and figure 7 gives time response examples. It is seen in both that the number of velocity peaks (extrema) to ± 10% of the magnitude of the first peak following a ground step disturbance without control is N_p = 29 whereas it is N_p = 3 with ϵ_o = 0.075 m/s (i.e., $\epsilon_{SR} = \epsilon_o/E_V$ = 8.3%, where E_V = 0.9 m/s is the amplitude of the first positive velocity peak without control) and that the number of valve openings in the latter case is N_V = 4. The valve does not always reach its fully-open position due to its dynamical limitations. For relative threshold velocities ϵ_{SR} less than 8.3%, the number of valve openings increases rapidly to infinity implying that the valve is continually activated by small velocity fluctuations. This excessive valve activity would be unacceptable in practice. On the other hand N_V decreases to [1,2] and N_p increases to

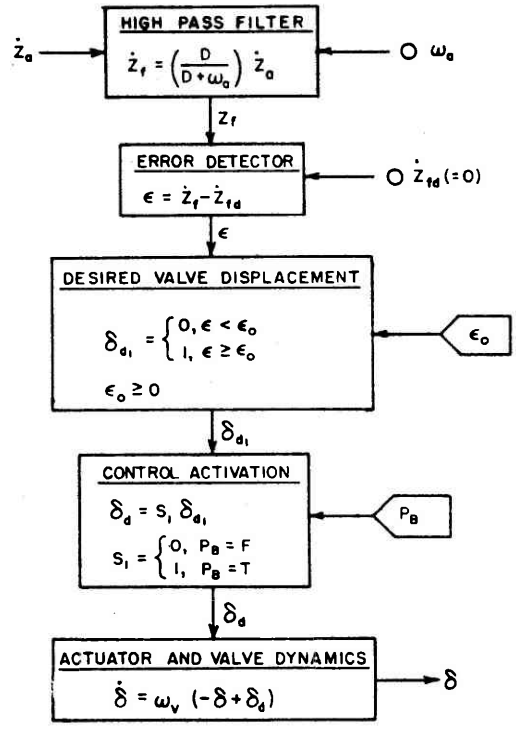


Fig. 2: Relay control information flow diagram

[6,9] for $\varepsilon_{SR} \in [30\%, 100\%]$. When $\varepsilon_{SR} > 100\%$, the system operates essentially without control since the valve is not actuated. Thus, depending on the desired compromise between velocity attenuation and valve activity, an optimum setting would be in the interval $\varepsilon_{SR} \in [8.3\%, 30\%]$.

Marginally Unstable System

The results presented in this section were obtained with a fan speed N = 2050 rpm such that the uncontrolled system was marginally unstable. Thus, since an unconditionally unstable system is a marginally unstable system whose unstable limit cycle amplitude tends to zero, the discussion is qualitatively general for unstable operation. The results presented in figures 5, 6 and 8 were obtained by first disturbing the system to establish a stable limit cycle without control and then activating the feedback control. The limit cycle velocity amplitude without control was $L_U = 0.75$ m/s and the effect of control was to reduce it to a controlled limit cycle velocity amplitude L_C. The relative limit cycle velocity amplitude is defined by $L_{CR} = L_C/L_U$.

Figure 5 shows that $L_{CR} = 0$ for $\varepsilon_o \in [0.025, 0.125]$, i.e., the relative limit cycle threshold velocity $\varepsilon_{LR} = \varepsilon_o/L_U$ in the interval [3.33%, 16.67%]. In this same interval, the number of valve openings N_{VT} in transience from uncontrolled to controlled limit cycles decreases monotonically from 11 to 4 while the number of transience velocity cycles N_{CT} increases from 4 to 6. Therefore, the maximum threshold velocity capable of forcing the trajectory into the stable region of the phase plane is $\varepsilon_o \simeq 0.125$ m/s, or $\varepsilon_{LR} \simeq 6.67\%$, and this setting yields minimum valve action. The value of L_{CR} increases monotonically to 33% for $\varepsilon_{LR} \in (16.67\%, 40\%]$, indicating that the threshold velocity is not small enough to force the system into its stable region but the stable limit cycle amplitude is reduced. The controlled limit cycle is maintained at a diminished amplitude by cyclical valve operation, the frequency of which can be characterized by the number of velocity cycles per valve opening $N_{C/V}$. It is seen that $N_{C/V}$ decreases monotonically from 3 to 1 in the interval $\varepsilon_{LR} \in [20\%, 40\%]$. Thus, the inverse relationship between L_{CR} and $N_{C/V}$ in this interval is fortunate since it indictes that valve activity is reduced as the controlled limit cycle amplitude is reduced. For $\varepsilon_{LR} > 100\%$, the system is effectively uncontrolled; therefore,

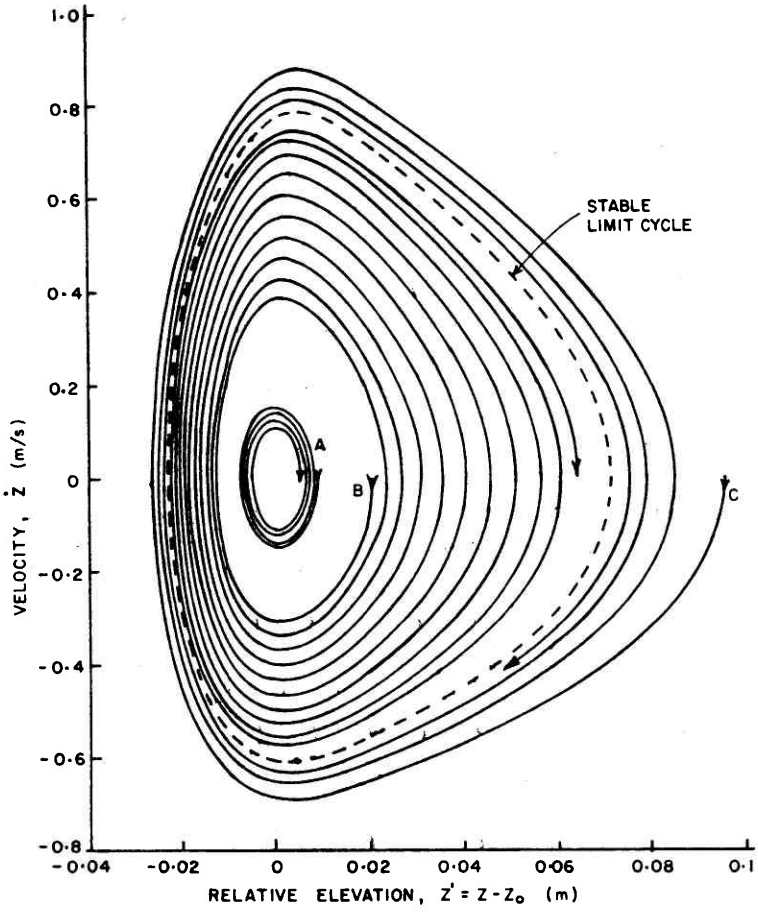


Fig. 3: Phase plane trajectories

L_{CR} = 100% whereas $N_{CT} = N_{VT} = 0$, but $N_{C/V}$ is a meaningless quantity since the valve is not activated. The system was not tested in the interval $\epsilon_{LR} \epsilon$ (40%, 100%].

It is seen from figure 6 that proportional control stabilizes the system for a wide range of control gain values, i.e., $K_P \epsilon$ [1, 10], and N_{CT} decreases monotonically in the corresponding interval $N_{CT} \epsilon$ [18.5, 2.5]. Furthermore, there is no residual limit cycle.

Limit cycle attenuation time responses are shown in figure 8 for (a) relay control with ϵ_o = 0.075 m/s, or ϵ_{LR} = 10%, (b) relay control with ϵ_o = 0.175 m/s, or ϵ_{LR} = 23.3%, and (c) proportional control with K_P= 8. The difference in valve activity between figures 8(a) and 8(c) is practically negligible but proportional control keeps the final velocity more steadily constant at a value of zero than relay control which is inactive in this region. Figure 8(c) illustrates the residual controlled limit cycle obtained with a larger threshold velocity and the two velocity cycles per valve actuation.

CONCLUSION

The following conclusions pertain to computer results from a typical air cushion heave dynamics model but can be qualitatively extended to other systems describable by structurally similar conceptual models.

The existence and amplitude of stable and usntable limit cycles is strongly dependent on airflow; hence, fan speed. The latter limit cycle is completely surrounded by the former and defines the region of stability in the phase plane.

Relay control can improve dymamic performance significantly without excessive valve action provided the system exhibits a sizable region of stability. On the other hand, proportional control is easier on hardware, is less dependent on stability region size and reduces the magnitude of residual motion.

Experimental studies[3] have qualitatively confirmed these conclusions.

NOMENCLATURE

A dot over a variable denotes the derivative with respect to time.

Roman

- D - Time differential operator
- E_V - Amplitude of first positive velocity peak during ground step down test without control
- F - Logical state 'false'
- K_P - Proportional control gain
- L_{CR} - Controlled relative to uncontrolled limit cycle velocity amplitude (peak-to-peak)
- L_U - Uncontrolled stable limit cycle velocity amplitude (peak-to-peak)
- N_{CT} - Number of transience velocity cycles from uncontrolled to controlled limit cycle
- $N_{C/V}$ - Number of velocity cycles per valve opening with controlled limit cycle
- N_P - Number of velocity peaks (extrema) to ± 10% of first peak following a ground step

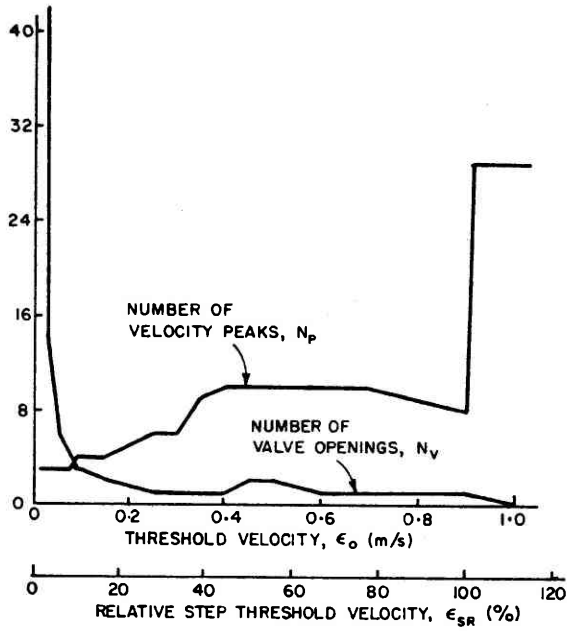


Fig. 4: Step response attenuation and valve activity as a function of threshold velocity

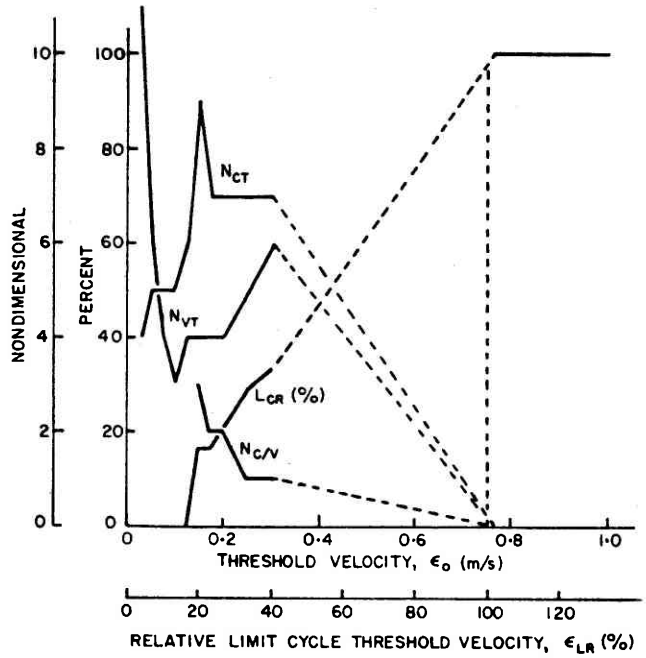


Fig. 5: Limit cycle attenuation and valve activity as a function of threshold velocity

N_V - Number of valve opening events following a ground step

N_{VT} - Number of valve opening events in transcience from uncontrolled to controlled limit cycle

P_B - Logical variable determining the 'on' or 'off' status of the control system

S_1 - Control activtion integer variable

T - Logical state 'true'

Z - Elevation of supports relative to ground

Z_a - Distance of supports from inertial reference

$\dot{Z}_f$ - Velocity of high-pass filter output

$\dot{Z}_{fd}$ - Desired value of high-frequency velocities

Z_o - Constant value of Z during stable steady state hover operation

Z' - Elevation of supports relative to Z_o

Greek

δ - Actual vent valve setting

δ_d - Desired vent valve setting when control system is activated

δ_{d1} - Desired vent valve setting should control system be activated

ϵ - Difference between desired and actual high-frequency velocities; also, 'in the interval'

ϵ_{LR} - Threshold velocity relative to uncontrolled limit cycle velocity amplitude

ϵ_o - Threshold velocity

ϵ_{SR} - Threshold velocity relative to E_V

ω_a - High-pass filter break frequency

ω_v - Actuator and valve break frequency

ACKNOWLEDGEMENT

The author is grateful to G. vanBlokland for computer programming assistance.

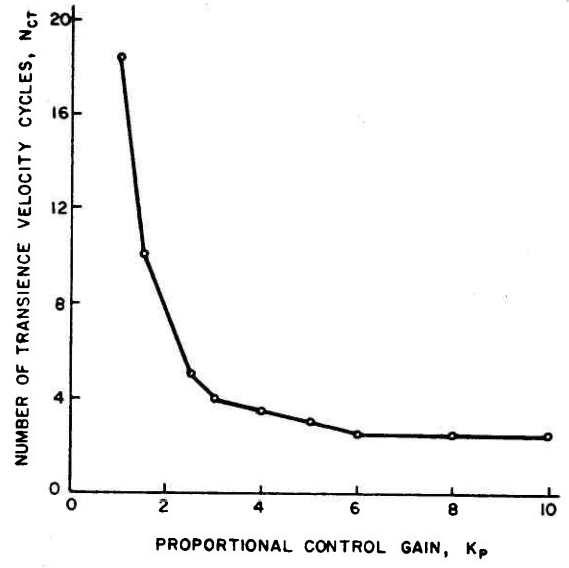


Fig. 6: Limit cycle attenuation as a function of proportional control gain

REFERENCES

1. Amyot, J.R., 'Computer Studies of ACV Heave Dynamics Stabilization', Proceedings of the 15'th Canadian Symposium on Air Cushion Technology, Toronto, Canada, September 1981.

2. Amyot, J.R., 'Computer Studies of ACV Heave Performance as a Function of Vent Valve Proportional Control Parameters', Canadian Aeronautics and Space Journal, Vol. 29, No. 1, March, 1983.

3. Amyot, J.R., Fowler, H.S., "An Experiment on Active Control of Air Cushion Heave Dynamics', Preprints of the 17'th Canadian Symposium on Air Cushion Technology, Ottawa, Canada, October, 1983.

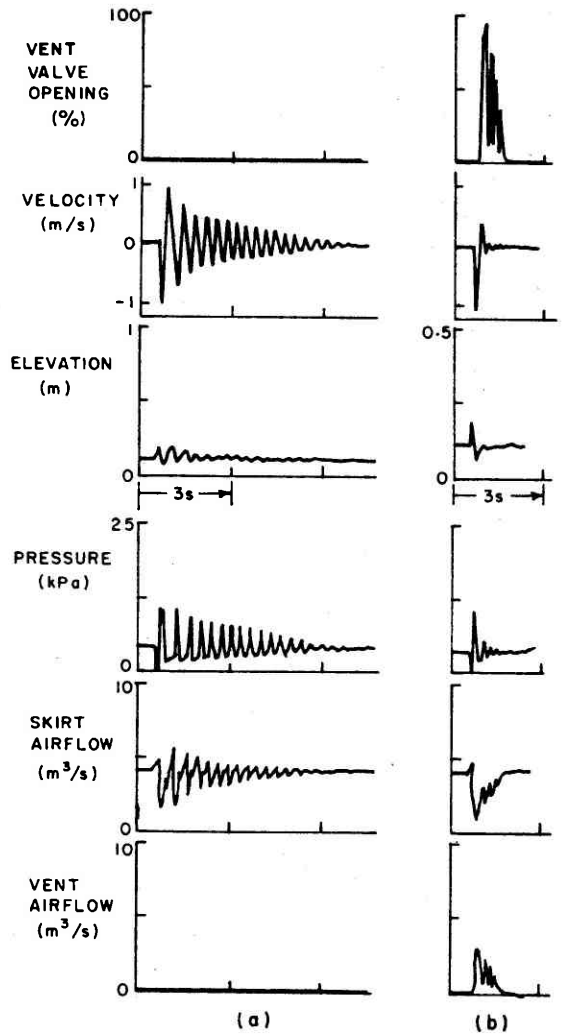


Fig. 7: Step disturbance time response; fan speed = 1625 rpm and hover elevation = 11 cm; (a) without control; (b) with control and ϵ_o = 0.075 m/s

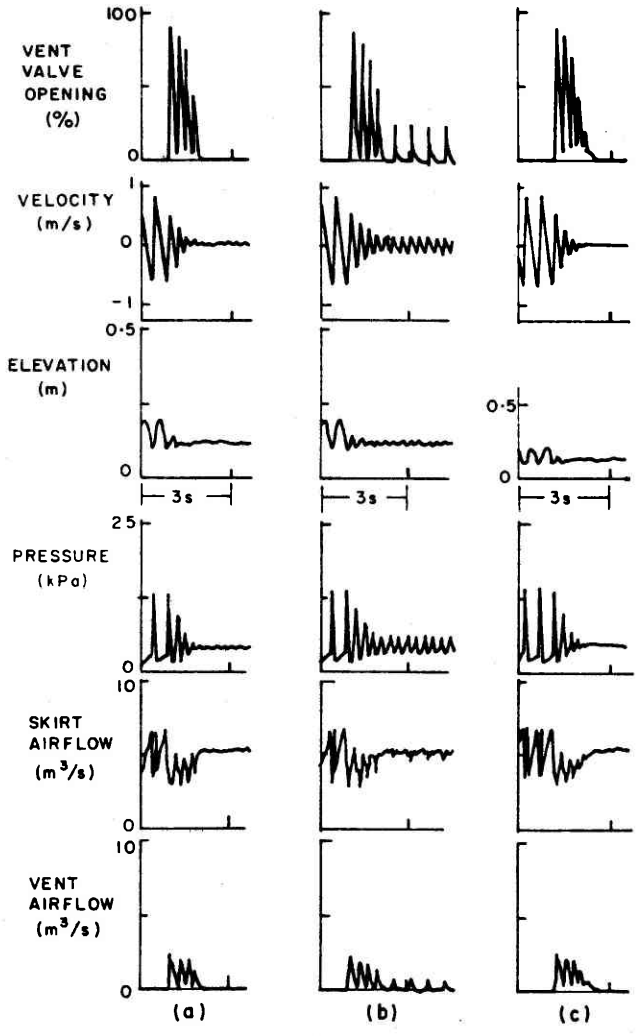


Fig. 8: Limit cycle attenuation time response; fan speed = 2050 rpm and hover elevation = 12 cm; (a) relay control with ε_o = 0.075 m/s; (b) ε_o = 0.175 m/s; (c) proportional control with K_p = 8

AN EXPERIMENT ON ACTIVE CONTROL OF AIR-CUSHION HEAVE DYNAMICS

J.R. Amyot & H.S. Fowler

National Research Council
Ottawa, Ontario

ABSTRACT

A physical model of an air cushion vehicle hull system, together with a ground board free to oscillate in heave, was built and tested. The model was fitted with a relay control system operating a vent valve, and experiments were carried out to validate and extend the insight into heave control gained from previously-reported studies on a hybrid computer system. Results here reported and discussed show that the system successfully controlled some regimes of heave, as predicted by the computer simulation.

INTRODUCTION

In references [1,2,3] Amyot described studies on a hybrid computer model to investigate the possibilities of controlling the heave oscillation of an air cushion vehicle (ACV). The present paper describes a physical experiment to validate the results obtained on the computer simulation, carried out in the Engine Laboratory, Mechanical Engineering Division, National Research Council of Canada.

The operation of a proportional control system was discussed in reference [1,2], while the simpler relay ("on-off") control was discussed in reference [3]. It was shown that the relay control could be fairly effective in some situations, but that the proportional control was more effective in general.

Since the relay control is simpler to build and operate, this was chosen for the initial experimental approach. The present paper presents the results of a physical experiment using a relay control system to attempt to stabilise a typical model ACV skirt in heave.

AIR CUSHION SYSTEM

One of the present authors had experienced heave oscillation on various ACVs, of up to 150 tonnes weight, and carried out experiments on a model in the laboratory. On the basis of this work, a test-rig for the present experiments was designed.

An actual ACV consists of a hull, on which is mounted a blower to provide air for lift, and propulsion machinery, cabin, etc. This hull is supported by the air cushion retained beneath it by a flexible "skirt" and the ground, and which is continually replenished with air by the blower.

However, such an arrangement in a model for heave experiments poses difficulties, since the instrumentation, blower, etc., would be too heavy to mount on the model, which needs to be tested over a range of weights. If these components are mounted on the ground and connected to the model by flexible lines, the mass and flexibility of these lines impose a very indeterminate restraint on the heave motion of the model.

It was therefore decided to invert and anchor the model ACV, whose air and instrument lines could then be made rigid, while the "ground" would be represented by a board supported above the model by the inverted air cushion. The "ground" would then oscillate freely in heave, and weights placed on it would simulate the vehicle weight by controlling the cushion pressure. The only assumption inherent in this inversion is that the gravitational forces on the inverted skirt are negligible compared to the aerodynamic forces on it. Since the skirt was made of 0.05 mm plastic sheet, this was considered justifiable.

In the light of these consideration, a test-rig was built as shown in the diagram of figure 1. The power unit was a centrifugal blower driven by a 1.1 kw electric motor. Since this was a constant-speed machine, the airflow to the rig was controlld by throttling the blower-inlet and opening or closing the bleed valve which was sited immediately downstream of the blower.

Since it was essential to measure the airflow entering the cushion, a long straight pipe was placed between the bleed valve and plenum, with a standard sharp-edged metering orifice in it. A pressure transducer enabled the pressure differential across this orifice to be used to calculate the lift-airflow.

Unfortunately the presence of the long duct was known to have a destabilizing effect on the skirt/plenum system heave characteristic (Ref. 5), but this was accepted as a constraint in the experiment, as was the presence of a specific blower characteristic. The air from the duct was discharged into the large plenum box which represented the hull of the inverted ACV. On

the top of this box was the model skirt, and above this, supported on the cushion of air, was the "ground-board". It was essential that this ground-board should be completely free to oscillate in heave, and at the same time not allowed to roll, pitch, or move sideways. It was therefore fitted with a vertical shaft on its centre, extending downward through an air-bearing. This arrangement was essentially frictionless, and possessed no inertia other than that due to the mass of the board and rod.

The skirt use was a simple, segment-only HDL type, with a circular footprint of 42 cms. diameter, a height from ground to upper hinge-point of 9 cms., and having 60 segments each of 1.6 cms. width. It was made of extremely flexible .05 mm thick transparent polyethylene sheet.

The cushion pressure could be varied by placing steel-sheet weights on the ground-board, whose total mass could thus be varied from 3.93 kg. to 15.90 kg.

The vent valve was a "venetian-blind" type, developed specifically for this application, and operated by an air-jack actuator. It consisted of five vanes, 20.5 cms. long, pivotted on their centrelines and moved by cams connected to a common bar moved by the air jack. The full aperture when open was 20.5 x 25.5 cms., obstructed only by the five edge-on vanes, each of 8 mm thickness. During the early experiments this opening was masked by progressively smaller orifices, until an 8.9 cm. diameter orifice was selected for the program.

There were doubts at the outset as to whether the valve would actually permit airflow during very short opening periods, with only 1 kPa pressure difference across it. The valve was constructed of the lightest possible material, to reduce its inertia, and perfect sealing was sacrificed to obtain a design capable of the fastest possible opening and closing. Since the natural frequency of heave of the system appeared to be approximately 3 Hertz, the simplest operating cycle appeared to be a "square wave", with instant opening and closing, and 0.15 sec successive open and closed periods. A mock-up valve was operated as nearly as possible in imitation of this cycle after filling the plenum with dense smoke, with the blower running, and good flow characteristics were observed. The actual valve was then built, and after considerable development of valve and actuator system excellent operation was achieved.

CONTROL SYSTEM

The heave oscillation of the system was sensed by an accelerometer mounted on the ground-board. The signal from the accelerometer was filtered to remove unwanted high-frequency trembling, and integrated to indicate velocity. When this velocity exceeded a preset threshold level, the vent valve was actuated to reduce the oscillation. This was achieved by the circuit shown in detail in fig. 2. After the accelerometer output passed through the low-pass filter to eliminate high-frequency noise it was integrated to give a velocity signal which was amplified. This signal was applied to a comparator whose threshold value could be set over the full range of velocities from + to -1.5m/s. When the input signal exceeded the set threshold value, normally about +0.3m/s, the solenoid valve was energized. This opened the heave-control vent valve. A similar chain of events closed the vent valve when the velocity fell below the threshold value again.

The threshold value, as noted above, was set at plus 1.3 m/s, where the positive sign indicates upward direction of the ground-board (or of the craft in the real-life case). This was done so that after the craft had reached the lowest point in the heave cycle and was starting to move again, the vent valve opened to reduce the lifting force, thus allowing gravity to reduce the oscillation. The vent was not opened during the downward part of the oscillation, because at that time a high cushion pressure was needed to arrest the falling craft, and stop the heave.

INSTRUMENTATION

The instrumentation scheme for the experiment is shown in Fig. 2. It consisted of four channels, whose outputs were displayedby a strip-chart recorder. One of the four channels, from the accelerometer mounted on the oscillating ground-board, also acted as the controller of the vent valve.

Channel 1 on the recorder was fed by signals from the plenum pressure transducer. This sensor was mounted inside the plenum, in one of the top corners, where it would be close to the skirt but shielded from the dynamic effects of air movement.

Channel 2 was connected to a transducer measuring the pressure difference across the standard sharp-edged orifice in the straight pipe from blower to plenum. The signal from this sensor therefore gave an indication of the airflow to the cushion. Its output was also displayed in digital form, to assist the operator in setting up required running conditions.

Channel 3 was connected to the output of the accelerometer on the ground-board, as already described. This enabled the heave velocity of the ground-board to be recorded.

Channel 4 received a signal from the comparator in the same circuit, so that when the comparator found that the velocity signal overpowered the preset threshold value and consequenty triggered the solenoid valve, this event was recorded. Channel 4 could therefore be regarded as showing the point at which the vent valve opened, and subsequently closed.

Since all four channels of data were recorded on the same chart, it was possible to relate the phasing of the heave motion itself, airflow, plenum pressure and vent-valve operation. By running the rig without the control operating, either with self-excited heave or by perturbing it by hand, the uncontrolled oscillation could be recorded. If the controlling circuit was then energized, the effectiveness could be assessed, and the number, extent, and phase of the vent-valve operations could be measured.

In future work, a second accelerometer will be placed on the ground-board, to give a record of acceleration, which will be recorded without integration, and a rotary potentiometer will be connected to the ground-board via a light swinging arm, to give a direct record of board position instead of having to deduce this from the velocity trace.

DISCUSSION OF RESULTS

The behaviour of the system in three stability regimes will be discussed, and the influence of the relay heave control system shown in each case.

In all three cases the threshold heave velocity was set at 0.3 m/s; one vent valve only, with an orifice of 8.9 cms. diameter, was used. And the mass of the ground-board plus weights was 15.90 kg. The difference between the three cases was the airflow. It is well-known in actual vehicle operation that heave can be induced by exceeding a critical lift airflow, and can be stopped either by reducing the lift airflow, by moving onto porous terrain, or by introducing a deliberate leak between skirt segments. The latter two actions do in fact reduce the effective lift airflow.

Case 1 (Figure 3)

In this case the airflow was adjusted to bring the system into Conditionally Unstable Equilibrium. This is a condition where the magnitude of a disturbance determines the stability of the response. A small disturbance will allow the system to stabilise after it, but a large-amplitude disturbance will result in the system going unstable and reaching its limit oscillation.

Three sets of traces from the chart recorder are shown. Trace (a) shows, on an expanded time-scale, the system oscillating in heave at its limit cycle. The three traces shown, display the phase relation between plenum pressure (0.04 to 1.24 kPa) and vertical velocity (-0.65 to +0.65 m/s), and the fact that the vent valve did not operate. The frequency was approximately 2.78 Hz. It is interesting and surprising that, owing to the combined cushion and ground-board dynamics, the ground-board did not reach its lowest position until 0.44 seconds after the cushion pressure had peaked.

Trace (b) shows, on a condensed time-scale, the result of applying vent-valve control to the system in limit cycle oscillation. A single vent-valve action was sufficient to bring the system into stable operation. The vertical velocity was reduced from $\mp$ 0.70 m/s (far above the threshold triggering value of 0.3 m/s) to about $\mp$ 0.1 m/s, and careful inspection shows that the triggering did take place in the upward (+0.3) motion. The computer simulation suggests that a proportional control would have reduced the final oscillation to an even lower level.

Trace (c) shows the result of a series of applied disturbances. These represent a series of sharp downward pushes, randomly delivered at different phases of the oscillation, at points A to F on the trace. It is seen that the system tended to destabilise, but that bursts of one, two or three valve actions brought the system back within bounds in every case.

Case 2 (Figure 4)

In this case the airflow was high enough that the system was in fully-developed Unconditionally Unstable Equilibrium. As figure 4(a) shows, control was switched on after the limit cycle had been established, and momentarily reduced the oscillation. However, since the system was unstable, the oscillation built-up again, requiring repeated operation of the vent valve. It is clear that while the vent valve was effective, the relay control system was not, and permitted repeated bursts of heave oscillation. This shows that a proportional control system would be essential to give a smooth ride on an unstable cushion system.

On the trace (b), plotted on an expanded time-scale, it is interesting to see that the length of the vent-valve's open period appears to be proportional to the rate of increase of vertical velocity at the moment of exceeding the threshold value. Higher rate of velocity increase might well be expected to result in a bigger overshoot during the valve-opening moments, and hence require a longer open period and consequent greater plenum pressure drop before the upward motion was arrested. Indeed this state of affairs is shown in the first and third valve operation. The second operation, in response to a slower rate of velocity rise, was of much shorter duration.

Case 3 (Figure 5)

This case shows an Underdamped Stable System, which was excited into oscillation by lifting and dropping the ground-board. The board was lifted sufficiently high that the air escape area between skirt and ground-board was large enough to drop the plenum pressure to zero. Since the system was stable, although underdamped, when the board was then dropped, it entered a damped oscillation which decayed to zero in a little over ten seconds. Trace 5(a) shows that it required 42 peaks of oscillation

before the amplitude decayed to 10% of the level of the largest peak. Trace 5(b) shows the performance of the same system with the vent-valve control switched on from the outset. The oscillation decayed to 10% in the much shorter time of 12 peaks in this case, showing the effectiveness of the relay control in dealing with strong perturbations of an underdamped stable system.

Trace 5(c) shows, on an expanded time-scale the reaction of the control system. The initial positive velocity represents the manual lifting of the ground-board. The vent-valve was actuated by this somewhat "spurious" signal, and the resulting complete loss of cushion pressure caused an unusually severe initial cushion collapse, and corresponding negative (falling) velocity. However, even after this very severe disturbance, only two valve openings restored stable equilibrium almost completely.

CONCLUSIONS

An experimental program has been carried out on a segmented cushion, using a relay control system to actuate a vent-valve to reduce heave oscillation. This system gave most encouraging results, and substantiated the predictions of the previous computer simulation. The substantiation must be classed as qualitative, since the physical model was not an exact reproduction of the geometry or blower characteristic simulated on the computer.

The existance of stable, conditionally stable, and unstable limit cycles with the same geometry but varying airflow values was demonstrated on the physical model, and seen to conform with full-size vehicle performance.

It was shown that the stability of a vehicle could be considerably improved by a relay-controlled vent-valve system, provided that a stable region exists within the craft's operating envelope.

Studies with the computer simulation show that a proportional control would be expected to have a better performance.

Additional instrumentation will be added to the test rig, and proportional and other control algorithms will be applied as the experimental program progresses.

ACKNOWLEDGEMENT

The authors wish to thank D.L. Bailey, L. Morriset, D. Matheson and R. Lowe for their assistance with the experimental program, and the Canadian Coast Guard for funding assistance.

REFERENCES

1. Amyot, J.R., "Computer Studies of ACV Heave Dynamics Stabilization", Proceedings of the 15th Canadian Symposium on Air Cushion Technology, Toronto, Canada, September 1981.

2. Amyot, J.R., "Computer Studies of ACV Performance as a Function of Vent Valve Proportional Control Parameters", Canadian Aeronautics and Space Journal, Vol. 29, No. 1, March, 1983.

3. Amyot, J.R., "Simulation of Air Cushion Heave Dynamics with Vent Valve Relay Control", Preprints of the 17th Canadian Symposium on Air Cushion Technology, Ottawa, Canada, October 1983.

4. Fowler, H.S., and Smith, R.R., "An Overwater Heave Experiment with Research Air Cushion Vehicle HEX-5, NRC report LTR-ENG-89, March 1979.

5. Hinchey, M.J., Sullivan, P.A., "Duct Effects on the Heave Stability of Plenum Air Cushions", Journal of Sound and Vibration, Vol. 60, No. 1, 1978.

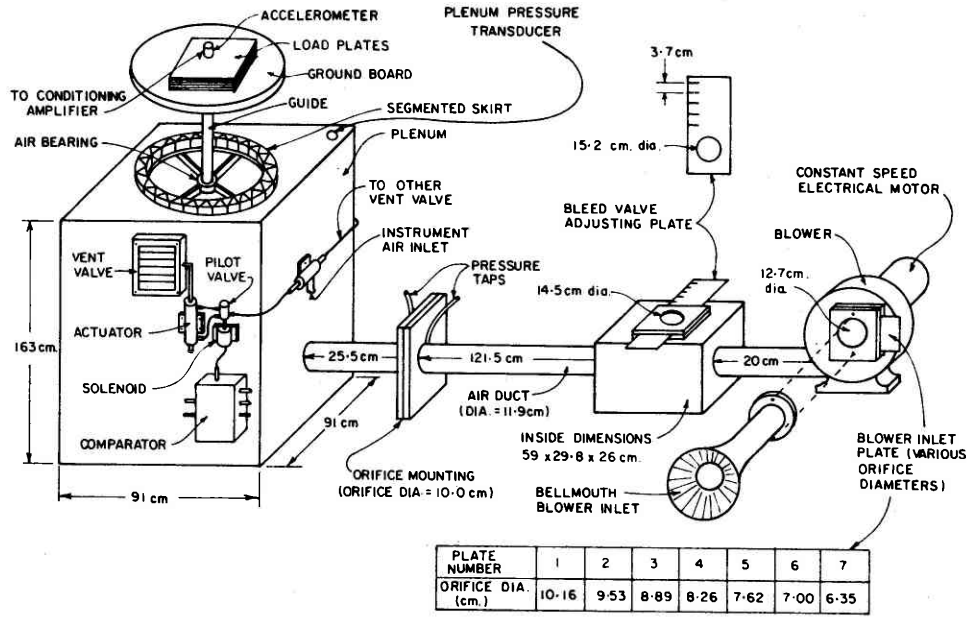


PLATE NUMBER	1	2	3	4	5	6	7
ORIFICE DIA. (cm.)	10·16	9·53	8·89	8·26	7·62	7·00	6·35

FIG. 1: Physical layout

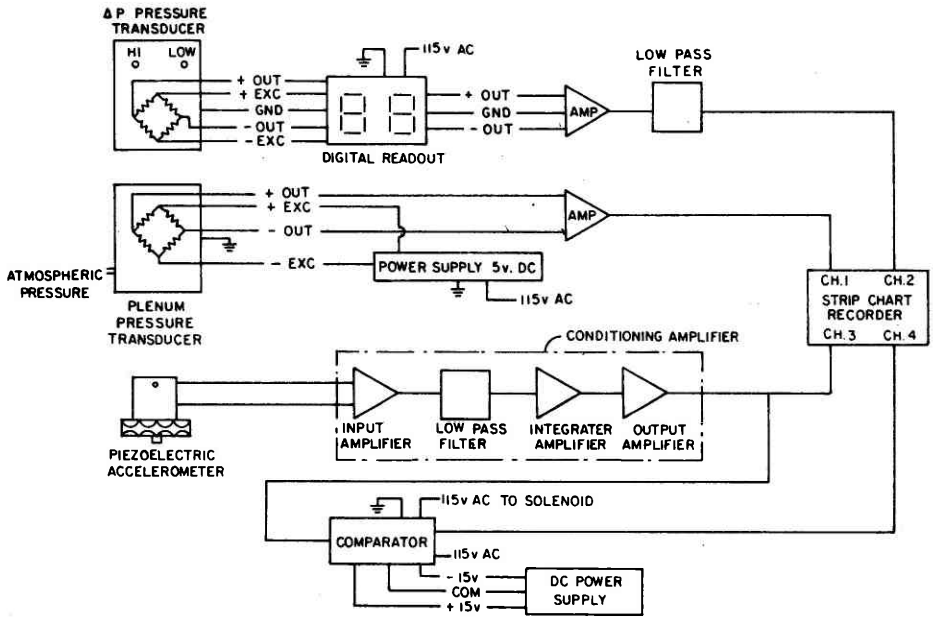


FIG. 2: Instrumentation

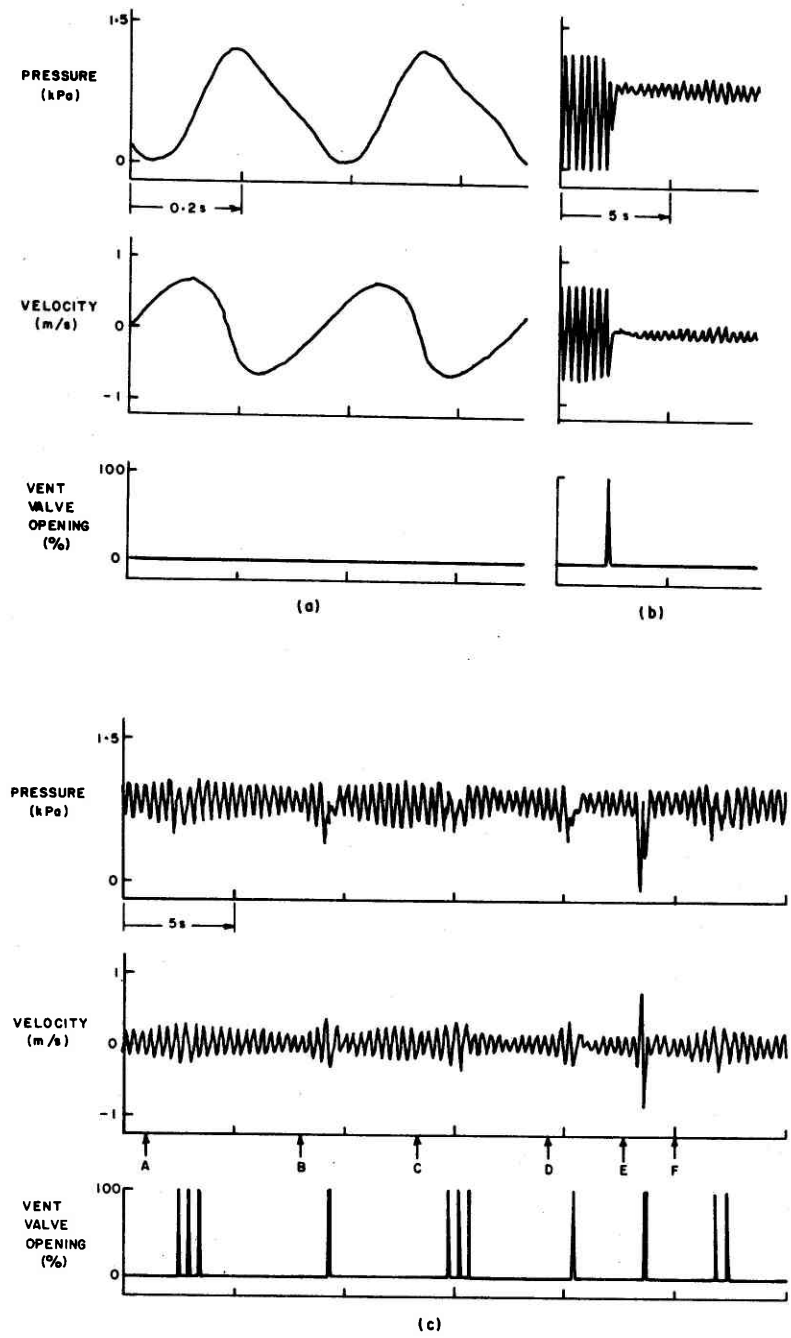


FIG. 3: Time responses of conditionally unstable system:
(a) Uncontrolled stable limit cycle
(b) Control applied during stable limit cycling
(c) Repeated downward manual impulses (A-F) on ground board

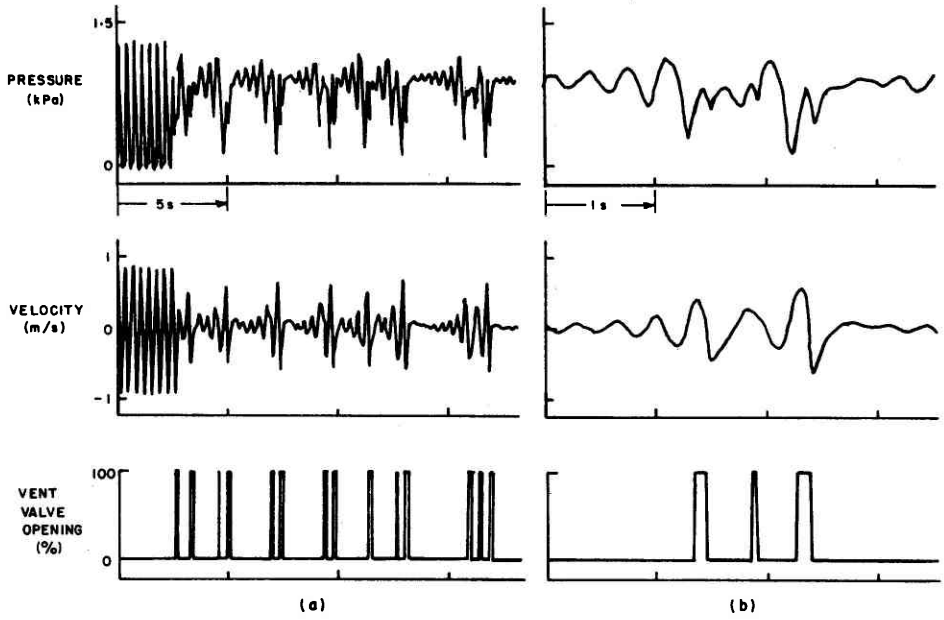


FIG. 4: Time responses of unconditionally unstable system:
(a) Control applied during stable limit cycling
(b) Continuation of (a) with expanded time scale

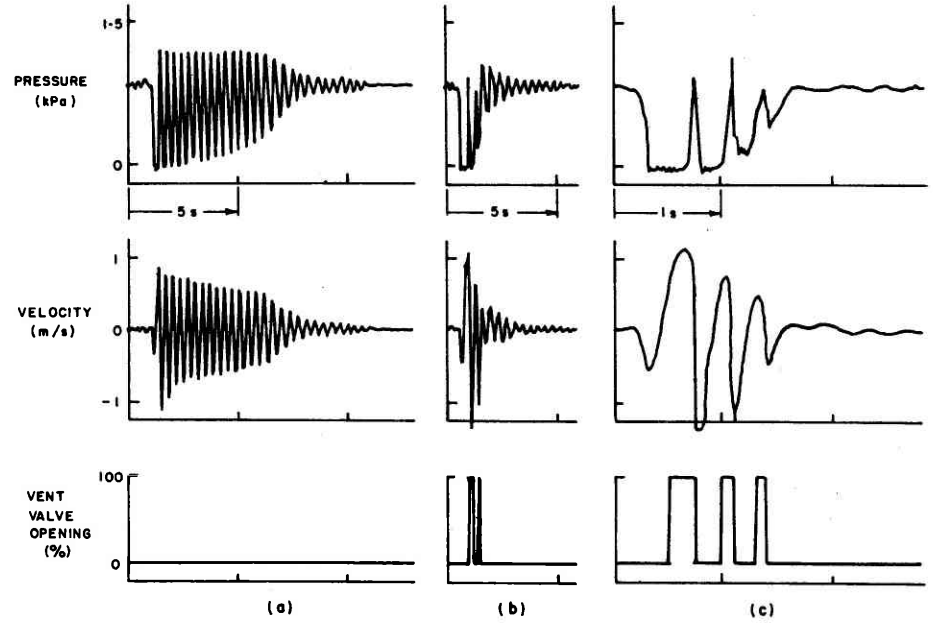


FIG. 5: Time responses of underdamped stable system upon dropping ground board from a 25 cm elevation:
(a) Without control
(b) With control
(c) With control and expanded time scale

HIGH SPEED AIR CUSHION ICEBREAKING
MEMBRANE ICE SHEET MODEL

M.J. HINCHEY

Faculty of Engineering and Applied Science
Memorial University of Newfoundland

ABSTRACT

This paper models an ice sheet as a membrane under tension and considers the waves generated by an air cushion vehicle moving over the sheet. It shows that there can be simultaneously two waves in the vicinity of a moving vehicle: one a stern wave similar to that seen over open water; the other a bow or precursor wave.

INTRODUCTION

An air cushion vehicle moving on its own over an ice sheet was first observed to break ice during the 1974 field trials of the CCG Voyageur (Figure 1). Observations indicated that it did this by setting up a large stern wave in the ice sheet. Since that time, several vehicle-ice interaction models have been developed.

The simplest model ignores the effect of the ice itself on the waves generated[1]. It can be found in most texts on classical hydrodynamics[2]. The most widely used but most often criticized model assumes the ice sheet to be a thin plate. This model was developed by Nevel[3] at C.R.R.E.L.. It predicts a critical or optimum speed for a given ice sheet. Shinbrot[4] recently argued that the plate model is flawed because it predicts a critical speed which is independent of the vehicle planform or weight. Others[5] apparently believe that the plate model predicts a wave pattern which is symmetrical fore and aft. This obviously doesn't occur in practice. So it has been argued that the plate model is of limited value.

The latter criticism is not justified. Although the plate model does predict a symmetrical pattern below the critical speed, above it the pattern predicted is asymmetrical. The objective of this paper is to prove this point. The plate model itself is not used. Instead, the closely related but simpler membrane model is utilized.

MEMBRANE ICE SHEET MODEL

This model is essentially an adaptation of that developed by Lamb[2] and others for studying the effect of a steady pressure disturbance on the surface of a running stream with capillary forces accounted for. As noted by Lamb[2], this model explains the fringe of ripples seen in front of a solid moving at a moderate speed through still water. Lamb's analysis is applicable here because capillary forces are effectively the same as those in a membrane under tension.

The analysis assumes the water to be deep and its motion to be two dimensional, incompressible and potential. Also, the wave pattern generated is assumed to be stationary relative to the disturbance, something observed experimentally. The bulk water motion must satisfy the conservation of mass law (see Figure 2)

$$\frac{\partial^2\phi}{\partial x^2} + \frac{\partial^2\phi}{\partial y^2} = 0 \qquad (1)$$

where ϕ is the velocity potential. It is also subject to the water surface kinematic condition

$$\frac{\partial\phi}{\partial y} = \frac{\partial\eta}{\partial t} \qquad (2)$$

and to the surface pressure condition

$$g\eta + \frac{P_b}{\rho} + \frac{\partial\phi}{\partial t} = 0 \qquad (3)$$

where η is the deflection of the water surface from its rest position and P_b is the pressure at the water surface. Newton's second law for the ice sheet gives

$$-T\frac{\partial^2\eta}{\partial x^2} - P_b + \sigma\frac{\partial^2\eta}{\partial t^2} = -P \qquad (4)$$

where T is the ice sheet membrane tension, σ is the sheet density per unit length and P is the moving pressure distribution. For a moving line of pressure (see Figure 3) Fourier transform techniques applied to the above equations yield

$$\hat{\eta} = \frac{-P_o}{(Tk^2+\rho g) - \rho c^2 k - \sigma c^2 k^2} \qquad (5)$$

where $\hat{\eta}$ is the Fourier transform of the ice deflection, k is the wave number, c is the line speed and P_o is a measure of the applied pressure. Letting

$$T^* = T - \sigma c^2 \qquad (6)$$

be an effective tension, the $\hat{\eta}$ equation reduces to

$$\hat{\eta} = \frac{-P_o}{T^*k^2 - \rho c^2 k + \rho g} \qquad (7)$$

The inverse Fourier transform applied to this gives the ice displacement. Above a certain speed, there are two singularities in the $\hat{\eta}$ equation. These dominate the generated wave pattern. When inversed Fourier transformed, they become respectively a short wavelength bow wave and a longer wavelength stern wave.

For a uniform distribution of pressure extending from x = 0 to x = ∞ an extension of Lamb's moving line analysis gives for x>0 the deflections

$$\eta = \frac{P_o}{\pi T^*}\left[\frac{2\pi \cos\kappa_1 x}{(\kappa_2-\kappa_1)\kappa_1} - \frac{E(\kappa_1 x)+\pi}{(\kappa_2-\kappa_1)\kappa_1} + \frac{E(\kappa_2 x)+\pi}{(\kappa_2-\kappa_1)\kappa_2}\right] \quad (8)$$

and for x<0 the deflections

$$\eta = \frac{P_o}{\pi T^*}\left[\frac{2\pi \cos\kappa_2 x}{(\kappa_2-\kappa_1)\kappa_2} + \frac{E(-\kappa_1 x)}{(\kappa_2-\kappa_1)\kappa_1} - \frac{E(-\kappa_2 x)}{(\kappa_2-\kappa_1)\kappa_2}\right] \quad (9)$$

where P_o is the level of uniform pressure, κ_1 is the stern wave number, κ_2 is the bow wavenumber, and where

$$E(\kappa x) = \left[\frac{\pi}{2} - S_i(\kappa x)\right]\cos\kappa x + C_i(\kappa x)\sin\kappa x \quad (10)$$

and

$$\kappa_2 = \frac{c^2\rho}{2T^*} + \sqrt{\left(\frac{c^2\rho}{2T^*}\right)^2 - \frac{g\rho}{T^*}} \quad (11)$$

$$\kappa_1 = \frac{c^2\rho}{2T^*} - \sqrt{\left(\frac{c^2\rho}{2T^*}\right)^2 - \frac{g\rho}{T^*}} \quad (12)$$

The deflections for a uniform distribution extending from x=L to x=∞ can be obtained from the above by substituting x-L for x throughout. The deflections for a two dimensional approximation of an air cushion (uniform distribution extending from x=0 to x=L) can be obtained by subtracting the x=L to x=∞ set of deflections from the x=0 to x=∞ set.

Note that infinite deflections result when $\kappa_1 = \kappa_2$. The latter occurs when

$$\left(\frac{c^2\rho}{2T^*}\right)^2 - \frac{g\rho}{T^*} = 0 \quad (13)$$

This gives the critical speed

$$c^4 = \frac{4T^*g}{\rho} = 4\,\frac{(T-\sigma c^2)}{\rho}\,g \quad (14)$$

and the associated critical wavenumber and wavelength

$$\kappa^2 = \frac{\rho g}{T^*} \qquad \lambda = \frac{2\pi}{\kappa} \quad (15)$$

Substitution into the $\hat{\eta}$ equation shows that at the critical speed tension and gravity forces are of the same order. One will also note that the ice density appears only indirectly through T^*. Setting it to zero does not eliminate the instability. However, it cannot be ignored because if $c^2 > T/\sigma$, $T^*<0$. A membrane cannot support compression; so if $c^2>T/\sigma$, the sheet would wrinkle and be structurally unstable.

The analysis shows that the deflection is finite above and below the critical speed. This suggests that the underlying phenomena is a resonance. In a reference frame moving with the disturbance the water moves as a current. Some insight can be obtained by considering the stability of an ice sheet floating on such a current as shown in Figure 4. The governing equations are

Conservation of Mass

$$\nabla^2\phi = 0 \quad (16)$$

Water Surface Constraints

$$\frac{\partial\phi}{\partial t} + U\frac{\partial\phi}{\partial x} + \frac{P_b}{\rho} + g\,\eta = 0 \quad (17)$$

$$\frac{\partial\eta}{\partial t} + U\frac{\partial\eta}{\partial x} = \frac{\partial\phi}{\partial y} \quad (18)$$

Ice Sheet Motion

$$\sigma\frac{\partial^2\eta}{\partial t^2} = P_b + T\frac{\partial^2\eta}{\partial x^2} \quad (19)$$

By assuming propagating waves of the form

$$\eta = \eta_o e^{i(kx-\omega t)} \quad (20)$$

$$\phi = \phi_o e^{ky} e^{i(kx-\omega t)} \quad (21)$$

one obtains the wavelength dispersion relationship

$$\omega = \frac{-B \pm \sqrt{B^2 - 4AC}}{2A} \quad (22)$$

where

$$A = 1 + k\frac{\sigma}{\rho}$$

$$B = -2Uk \quad (23)$$

$$C = -k\left(\frac{Tk^2}{\rho} + g\right) + U^2k^2$$

Substitution into the assumed forms shows that the propagating waves would grow in amplitude if

$$B^2 - 4AC < 0 \quad (24)$$

This gives the wavenumber dependent critical speed

$$U_f = \sqrt{\left(\frac{Tk^2}{\rho} + g\right)\left(\frac{\rho}{\sigma} + k\right)/k} \quad (25)$$

When $\sigma = 0$, $U_f = \infty$. Thus the infinite deflections noted earlier are not wave amplitude growth as discussed above. When C = 0, no information can propagate upstream against the fast moving current. This occurs when

$$U_d^2 k = \frac{Tk^2}{\rho} + g \quad (26)$$

The upstream wave does not propagate and is critically stable because $\omega=0$. The minimum in the U_d versus k relationship gives

$$U_d^4 = \frac{4Tg}{\rho} \quad \text{or} \quad U_d = \sqrt[4]{\frac{4Tg}{\rho}} \quad (27)$$

which is identical to the critical speed given earlier. In the literature on flow-structure

interactions[6,7], U_d is known as the divergence speed while U_f is known as the flutter speed. So the instability appears to be a divergence.

For the above the water was assumed to be deep. When the water is shallow

$$\hat{\eta} = \frac{-P_o}{T^*k^2 + (\rho g - \frac{\rho c^2}{h})} \qquad (28)$$

where h is the water depth. This gives for any T^* the critical speed

$$c = \sqrt{gh} \qquad k = 0 \qquad (29)$$

which is the phase speed of shallow water waves. In other words it is the speed associated with hydraulic jumps.

WAVE PATTERNS

Typical wave patterns obtained for the ACT-100 (see Figure 5) modelled as a uniform distribution of pressure of length L are shown in Figures 6 to 8. Each of these figures is for a specific forward speed and each plot within a particular figure is for a specific ice tension. Forward speed is given nondimensionally as a Froude number $c/\sqrt{gL}$: ice tension is given as a fraction of the critical tension associated with a particular speed (σ=0). Each plot gives ice displacement versus horizontal distance; the displacement is nondimensionalized by the hydrostatic displacement and the horizontal distance is nondimensionalized by the vehicle length. The results for each Froude number show how the deflections increase in magnitude as the sheet tension approaches the critical value.

Figure 9 shows some preliminary results for a moving pressure point (see Figure 10). For these, damping had to be added to keep the deflections finite. Also, only the contributions of the singularities were accounted for. Results for a moving pressure patch (air cushion) could be obtained from an extension of this analysis.

DISCUSSION

Recent measurements by Beltaos[8] of lateral deflections in the immediate vicinity of a vehicle moving over an ice sheet are surprising not far from the above predictions. The measured patterns are shown in Figure 11. Note that the measurements indicate that below the critical speed the pattern is approximately symmetrical fore and aft. However, above the critical speed it is not.

At the critical speed the analysis predicts infinite deflections. There is nothing fundamentally wrong with this. The analysis is linear, so instability or resonance implies infinite deflections. In practice, nonlinearity and/or damping would keep the deflections finite. One source of nonlinearity ignored here is the convective term in the surface pressure condition. Also, the models developed to date ignore the energy dissipation associated with creep phenomena in the ice sheet and with the initiation and subsequent propagation of cracks.

Considering the structural complexity and wide variability of ice sheets, one might wonder if a model which can adequately predict ice sheet failure will ever be developed. Theories obviously need material properties to make predictions. On the other hand critical experiments with controlled ice models would provide considerable insights.

ACKNOWLEDGEMENTS

Certain references quoted were made available to the author by Jacques Laframboise of Transport Canada. The work was funded in part by NSERC and in part by the Office of Research at Memorial University (MUN). Dennis English, an Engineering student at MUN, helped with computer programming.

REFERENCES

1. Carter, D., "Mathematical Analysis of Ice Breaking by Air Cushion Platforms", Transport Canada (TDC), TP-1238, Sept. 1977.

2. Lamb, H., "Hydrodynamics", Dover Publications, New York, 1945. Articles 270, 271 and 272.

3. Nevel, D., "Moving Loads on a Floating Ice Sheet", C.R.R.E.L., Hanover, N.H., U.S.A., May 1970.

4. Shinbrot, M., "A Preliminary Analysis of Dynamic Ice Rupture by Hovercraft", Transport Canada (TDC), TP-2461, Jan. 1980.

5. NRCC Associate Committee on Air Cushion Technology, "Ice Breaking with Air Cushion Technology", Technical Report 3/75, p. 6, 1975.

6. Weaver, D.S. and Paidoussis, M.P., "On Collapse and Flutter Phenomena in Thin Tubes Conveying Fluid", Journal of Sound and Vibration, Vol. 50, pp. 117-132, 1977.

7. Matsuzaki, Y. and Fung, Y.C., "Nonlinear Stability Analysis of a Two Dimensional Model of an Elastic Tube Conveying a Compressible Fluid", Journal of Applied Mechanics, Vol. 46, pp. 31-36, 1979.

8. Beltaos, S., "Field Measurements on the Response of Floating Ice Sheets to Moving Loads", Canadian Journal of Civil Engineering, Vol. 8(1), pp. 1-8, 1981.

APPENDIX

Membrane and Plate Deflections near Critical Speed.

The membrane deflection - wavenumber relationship is of the form

$$\hat{\eta}_m \alpha \frac{C_m}{k^2 - a\,k + b}$$

A plate analysis gives a relationship of the form

$$\hat{\eta}_p \alpha \frac{C_p}{k^4 - A\,k + B}$$

The singularities of these expressions dominate the respective wave patterns. At a critical speed, two singularities are equal. Thus, at a critical speed, $\hat{\eta}_m$ becomes

$$\hat{\eta}_m \alpha \frac{C_m}{(k-\kappa_m)(k-\kappa_m)}$$

while $\hat{\eta}_p$ becomes

$$\hat{\eta}_p \alpha \frac{C_p}{\kappa_p^2\,(k-\kappa_p)(k-\kappa_p)}$$

By absorbing the κ_p^2 term in the latter into C_p, $\hat{\eta}_p$ further reduces to

$$\hat{\eta}_p \alpha \frac{C_p^*}{(k-\kappa_p)(k-\kappa_p)}$$

So near a critical speed both models should behave qualitatively the same.



Fig. 1 CCG Voyageur

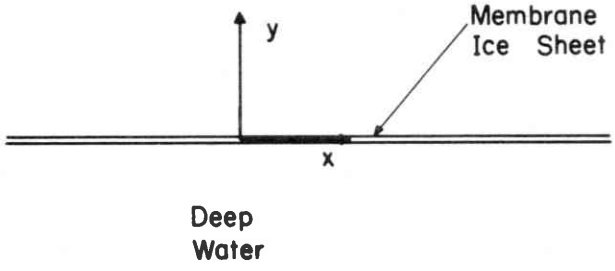


Fig. 2 Membrane Ice Sheet Model

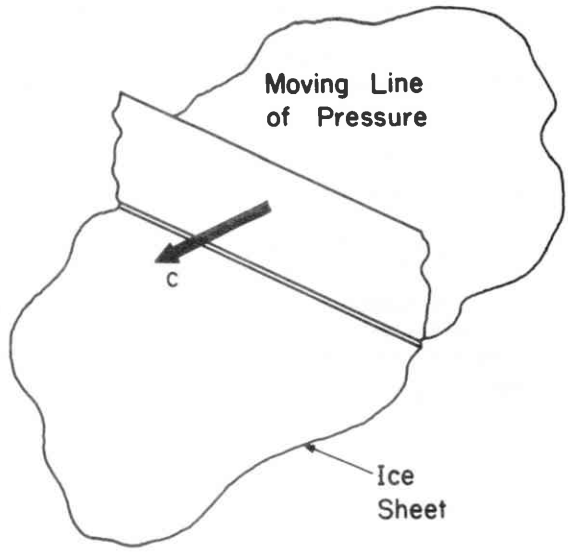


Fig. 3 Moving Line of Pressure

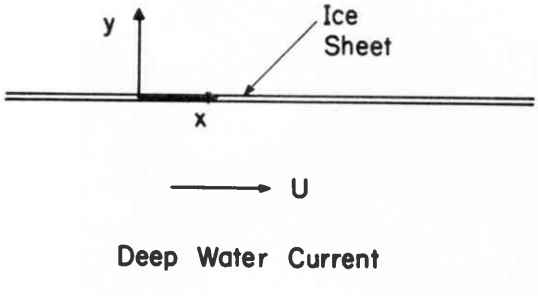


Fig. 4 Ice Sheet Floating on Fast Moving Current

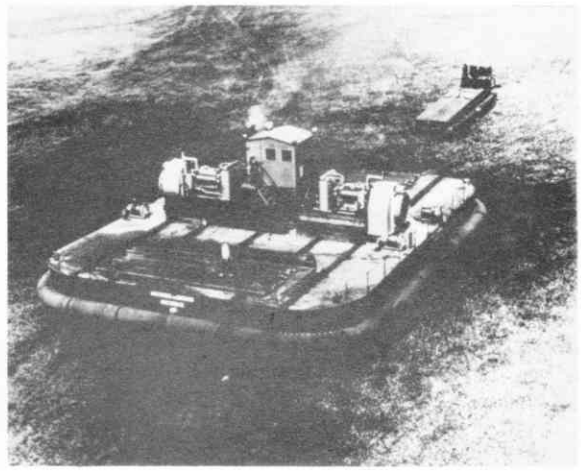


Fig. 5 ACT-100

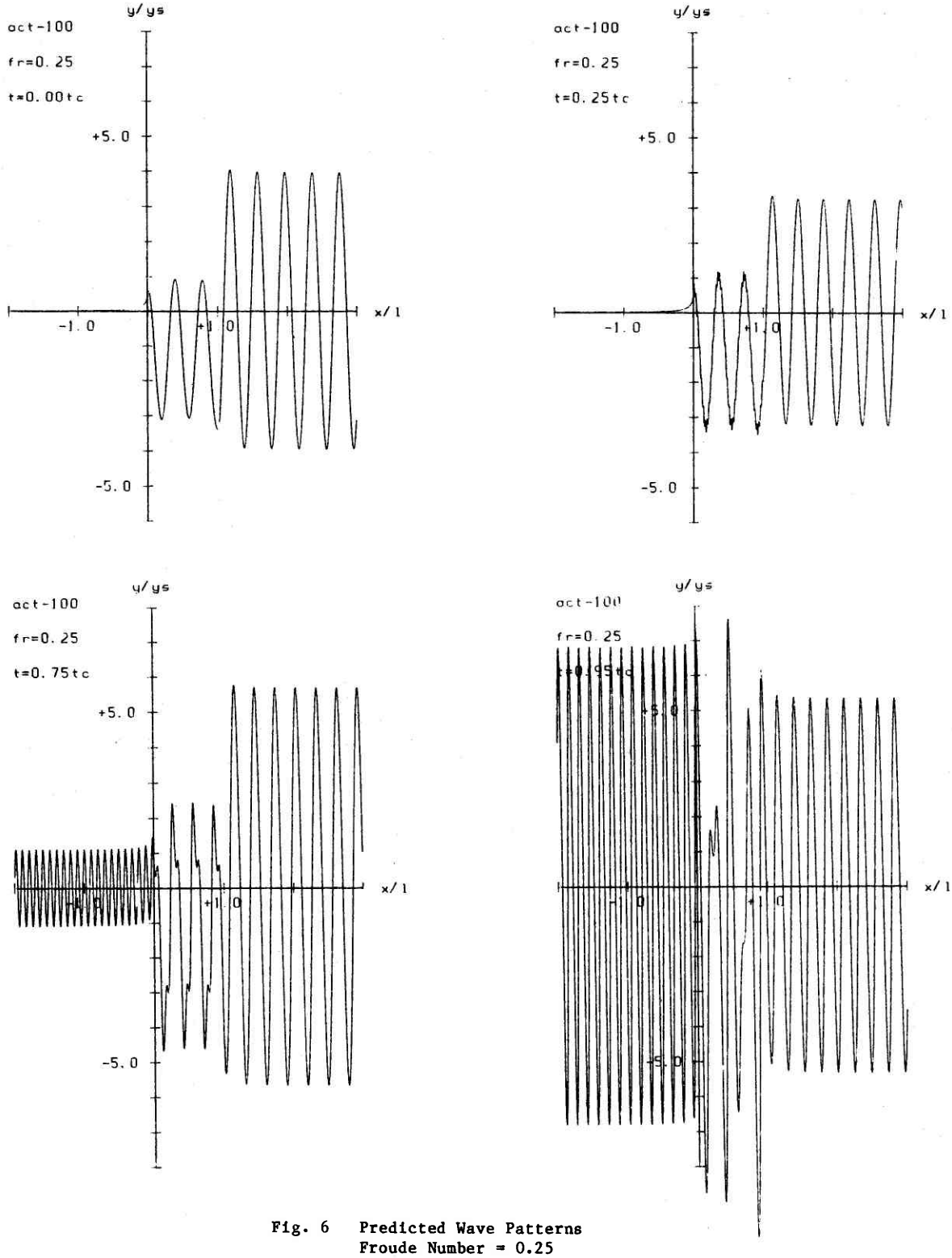
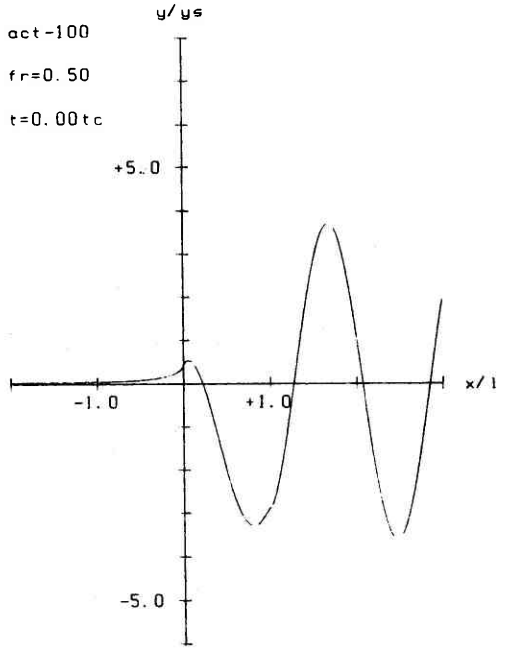
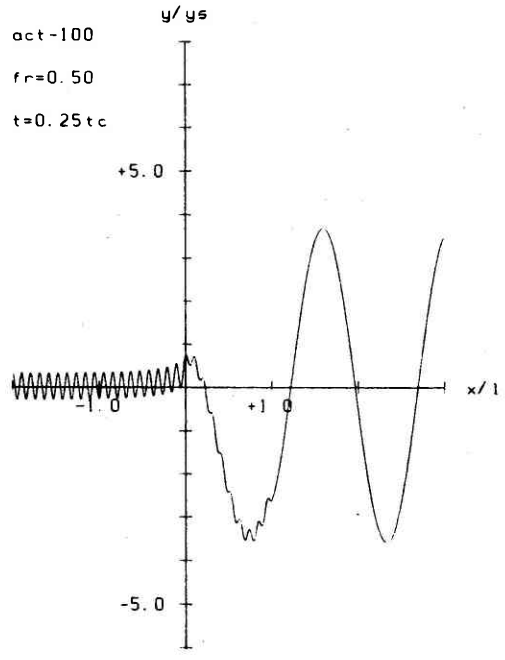
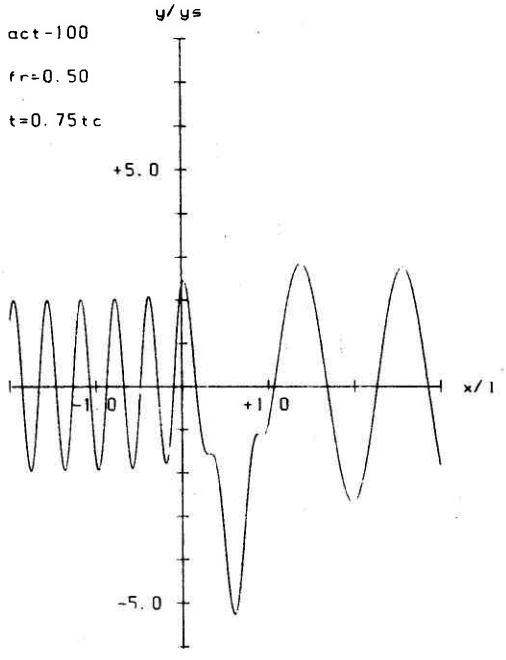


Fig. 6 Predicted Wave Patterns
Froude Number = 0.25







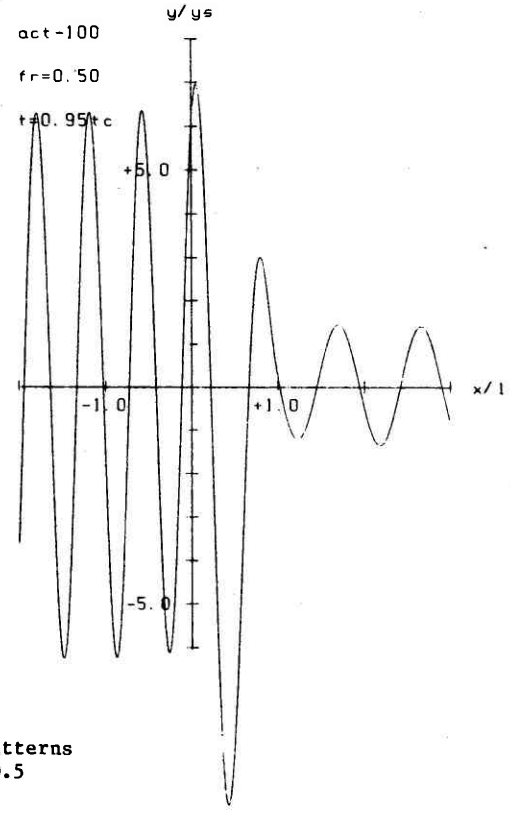


Fig. 7 Predicted Wave Patterns
Froude Number = 0.5

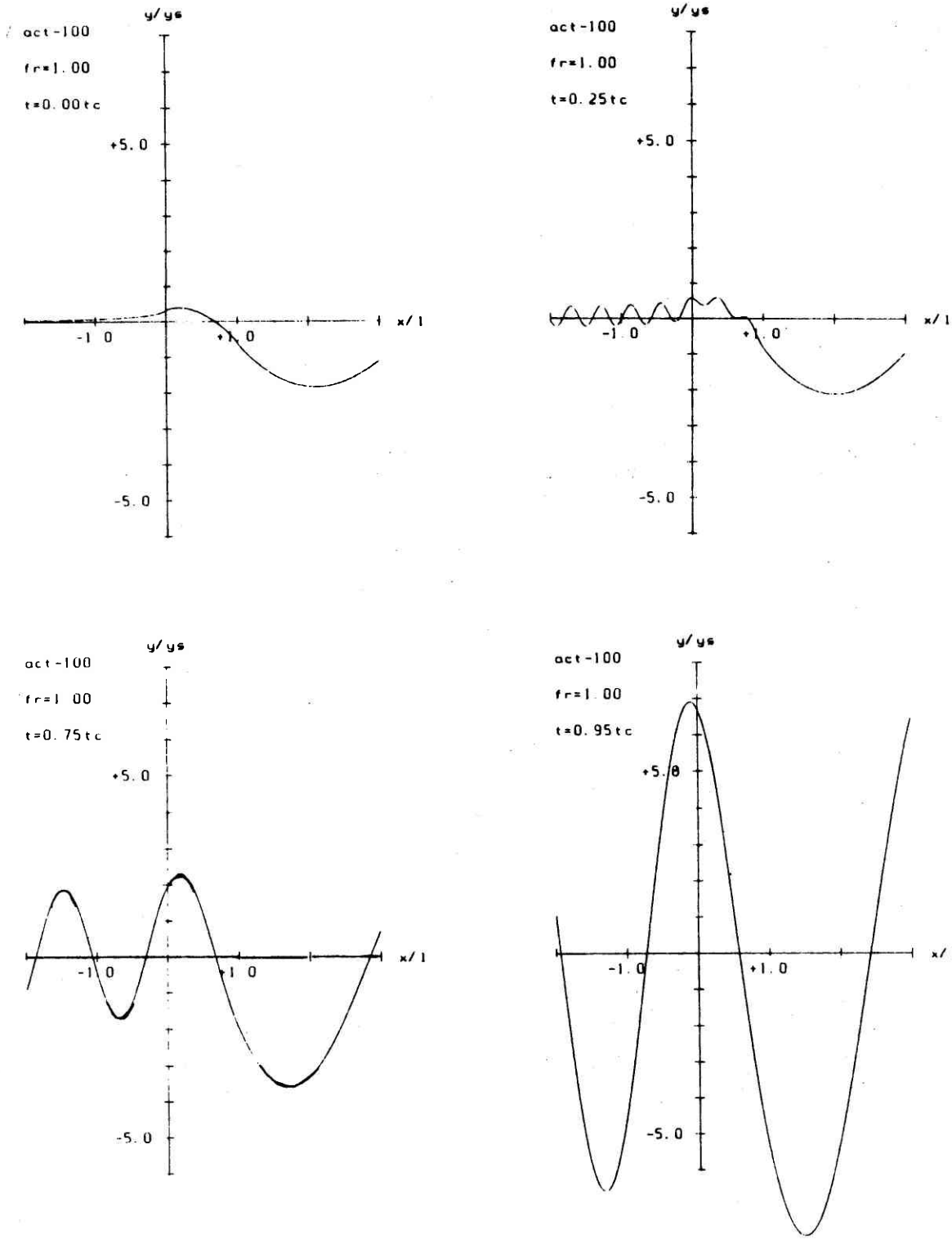


Fig. 8 Predicted Wave Patterns
Froude Number = 1.0

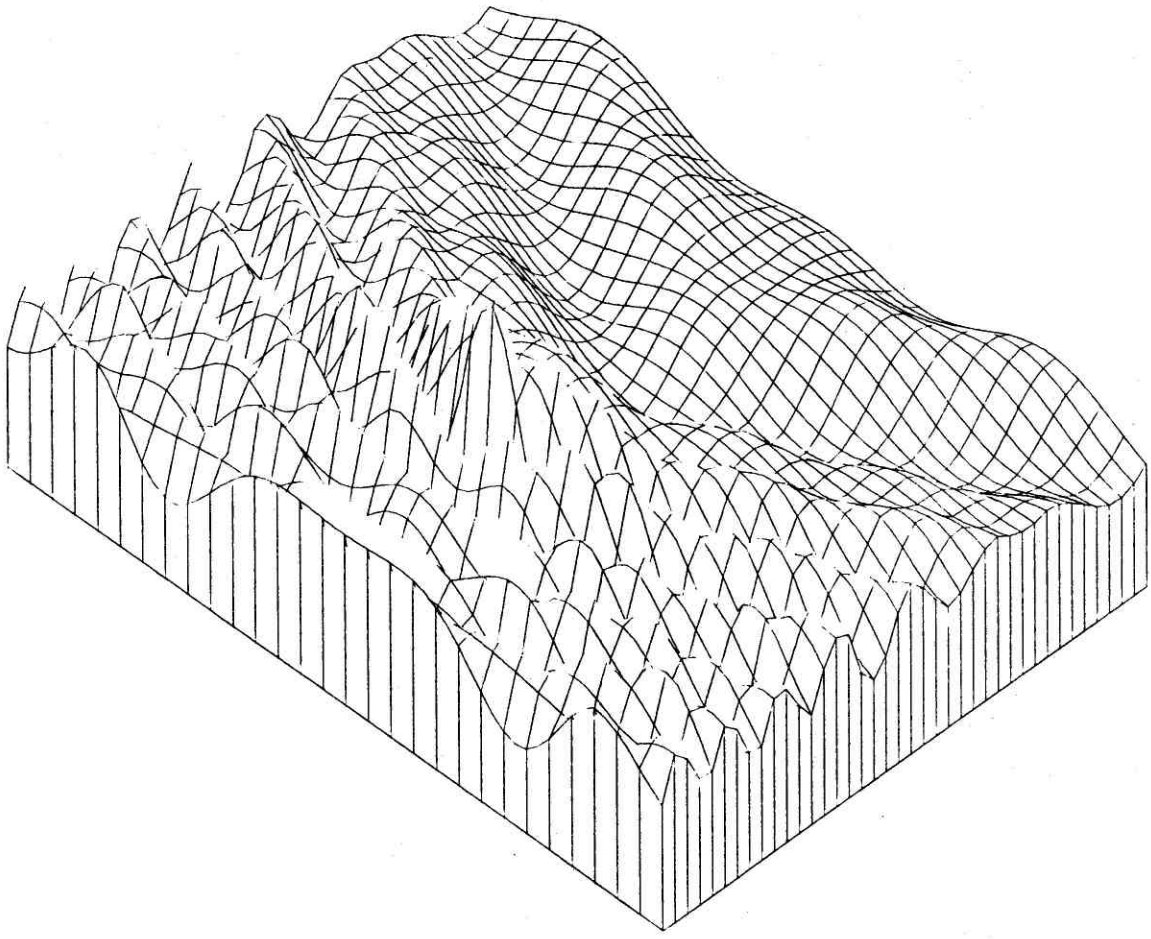


Fig. 9 Wave Pattern in Vicinity of Moving Pressure Point

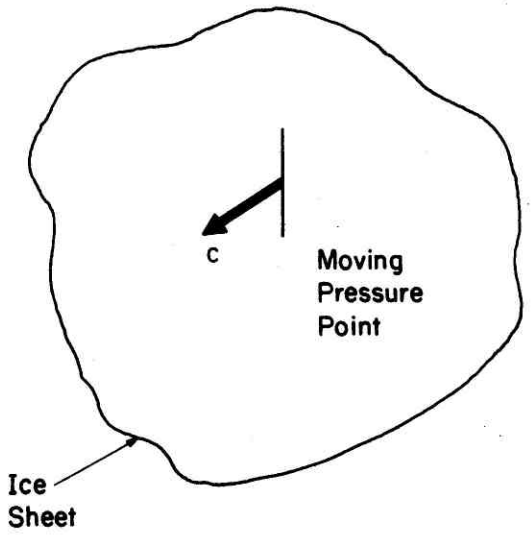


Fig. 10 Moving Pressure Point

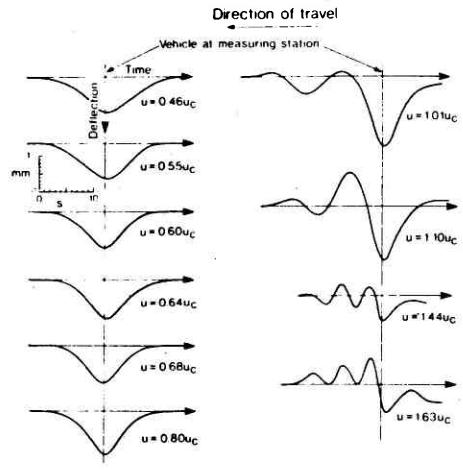


Fig. 11 Field Measurements by Beltaos

AN OVERVIEW OF CURRENT AIR CUSHION RESEARCH AT UTIAS

P.A. Sullivan

Institute for Aerospace Studies
University of Toronto

ABSTRACT

An overview of current air cushion research at the University of Toronto Institute for Aerospace Studies (UTIAS) is given. The following topics are discussed: (1) recently - obtained data on the effect of visco-elastic properties of skirt materials, (2) investigation of instability over water, (3) effects of hysteretic damping of skirt material on stability, (4) dynamic characteristics of centrifugal fans, (5) theoretical and experimental investigation of segmented - skirt cushions, and (6) sail-rail theory and practice.

HEAVE STIFFNESS HYSTERESIS MEASUREMENTS ON A LARGE SCALE AIR CUSHION

T. A. Graham,* P. A. Sullivan* and M. J. Hinchey†

*Institute for Aerospace Studies, University of Toronto
†Memorial University, Newfoundland

ABSTRACT

Data from the UTIAS Circular Track Project has shown that, at model scale, skirt hysteresis can be a major source of damping. In fact, when the model skirt has little hysteresis the test craft is often observed to self oscillate in combined heave-pitch-roll. In this paper, recent measurements of full scale hysteresis in a Canadian Coast Guard ice breaker bow platform (ACIB) skirt system are presented. These show that full scale hysteresis is comparable to that seen at model scale. An estimate of its effect on overall system damping is also presented.

INTRODUCTION

Model scale ACV testing at UTIAS has revealed that commonly used types of skirt systems exhibit hysteresis in their roll and pitch stiffness curves.[1-4] The hysteresis is associated with skirt-ground contact and the ability of the skirt material to sustain small compression loads. Cushion pressure measurements described in Ref. 4 indicate that the amount of load carried by the skirt is about 5% in some cases which would alter the moment coefficient by an amount of 1.5%. For segmented skirt designs roll and pitch hysteresis associated with skirt load carrying has been found to be typically in the order of 1% to 3% although it is effectively zero in some cases. In addition, it has been found to make a significant contribution to system damping in model tests.[3]



Fig. 1 Canadian Coast Guard air cushion ice breaker, "Iceater II".

An obvious question is, "Does significant hysteresis occur at full scale?" If it does, it represents an important source of damping that should be exploited. If it does not, then it suggests that skirt systems have not been scaled properly. This paper presents some full scale measurements of heave hysteresis in an air cushion ice breaker bow platform (ACIB), Fig. 1, currently being developed in Canada.

MODEL SCALE HYSTERESIS

Measurements of pitch and roll stiffness characteristics made on models at UTIAS indicate that hysteresis is present in both the segmented and multicell types of skirt design, as shown in Figs. 2 and 3.[1-4] Three different hysteresis mechanisms have been identified. Peculiar to multicell systems is a mechanism in which the downgoing cell would become shut off and then buckle and vent causing loss of support from that cell, Fig. 4. Sliding friction between the skirt and ground can also be a source of hysteresis as illustrated in Fig. 5 by the curves for the polyethylene film segmented skirt with the ground board fixed in one case but allowed to move in the other. Hysteresis also exists in the pressure vs pitch angle curves and the hysteresis for the polyethylene skirt, shown in Fig. 6, is more than twice that for a urethane-coated nylon fabric also tested. This indicates that the load-

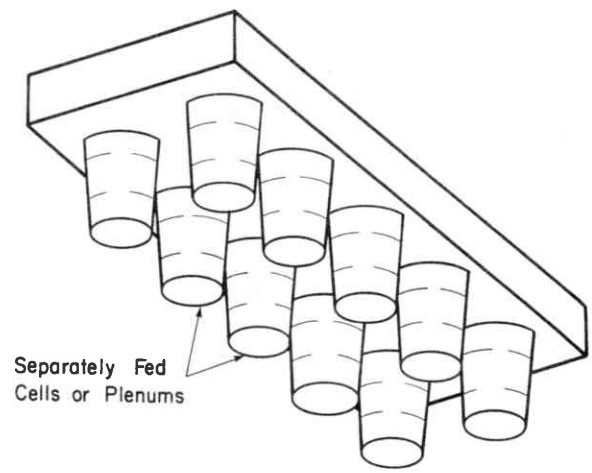


Fig. 2 Multicell cushion - schematic.

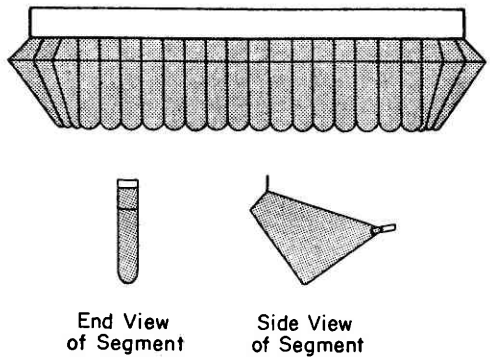


Fig. 3 Segmented-skirt cushion - schematic.

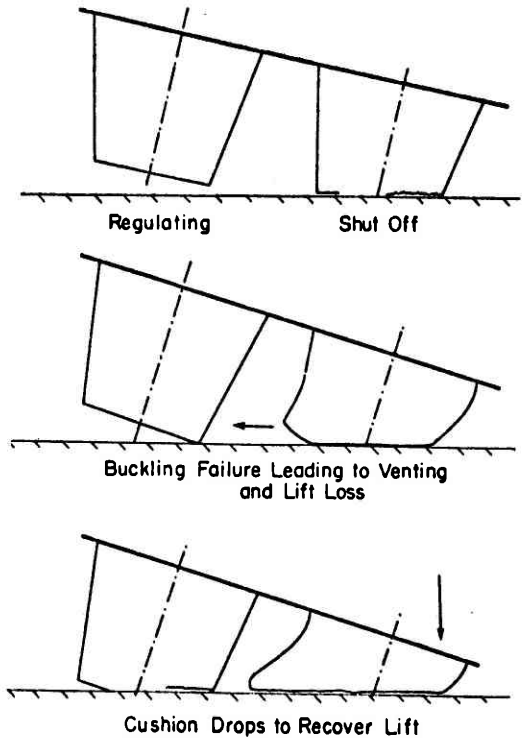


Fig. 4 Venting effects in multicell cushions.

carrying capability of the skirt is an important cause of hysteresis as well since the cushion pressure is determined by the footprint area, vehicle weight and the amount of load carried in the skirt and does not depend on friction. In some cases the friction is only a negligible component as with the nylon-urethane fabric in Fig. 5, where the shaded curve gives the fabric roll stiffness for both the moving ground fixed and free conditions. Note also the large increase in the amount of hysteresis occurring in the polyethylene skirt over the nylon-urethane skirt. This is shown even more dramatically in the pitch characteristics, Figs. 7 and 8. One further piece of information showing that the frictional component of the hysteresis is of secondary importance is the effect of varying cushion gross weight on the roll stiffness

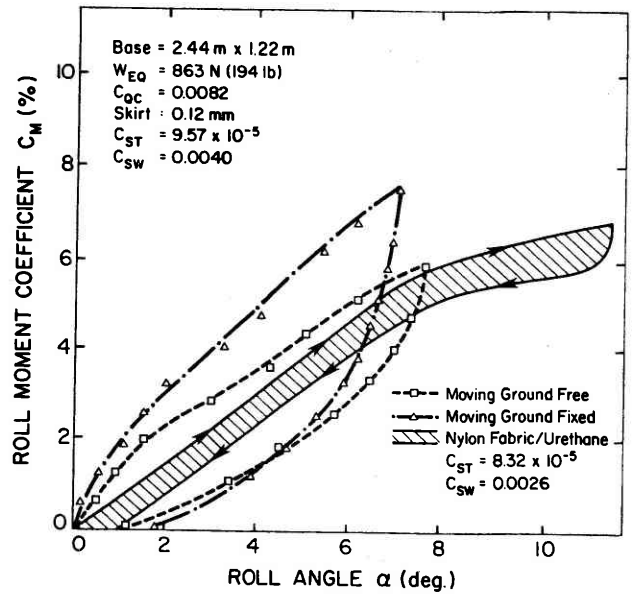


Fig. 5 Roll stiffness characteristic of cushion dynamics model equipped with HSL skirt including the effect of skirt-ground friction. Skirt material is polyethylene film.

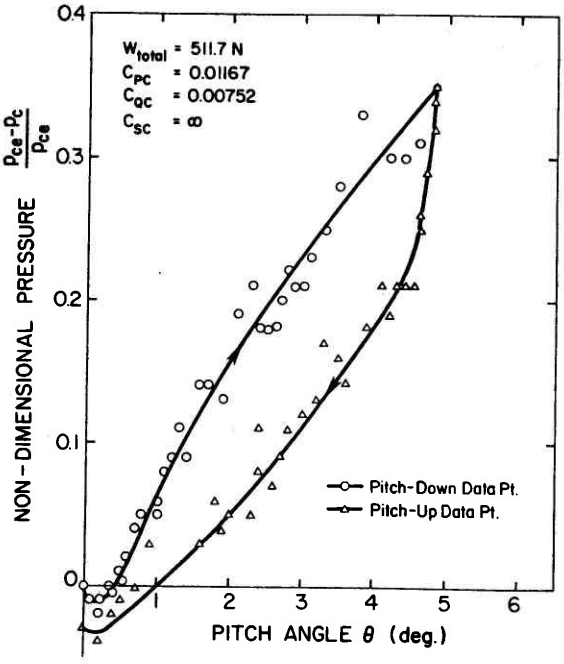


Fig. 6 Nondimensional pressure versus pitch angle θ, for the cushion dynamics model equipped with the polyethylene HSL skirt.

curves, Fig. 9. Here the reduction in size of the hysteresis can be due only to structural effects as the friction forces would increase proportionally with the gross weight because the normal

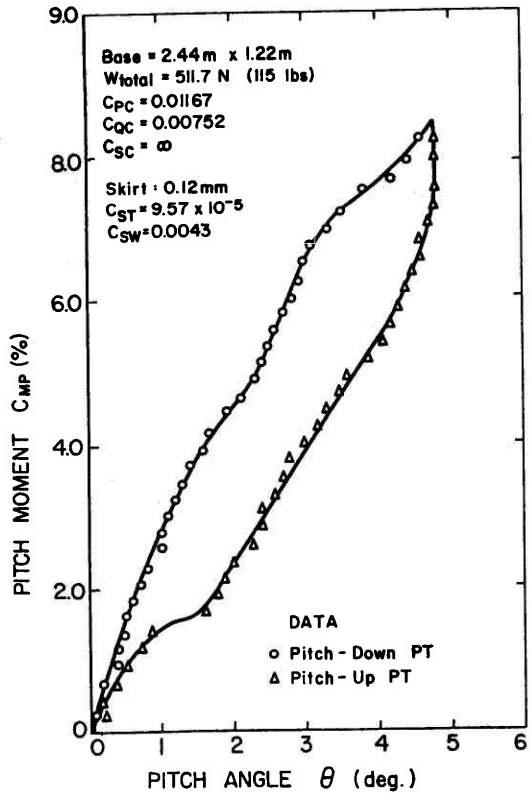


Fig. 7 Experimental pitch stiffness measurements for the cushion dynamics model equipped with the polyethylene HSL skirt.

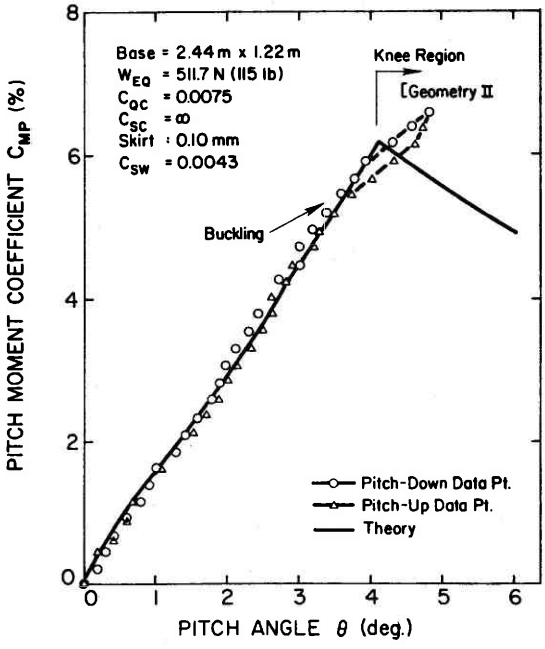


Fig. 8 Theoretical and experimental values of pitch stiffness of cushion dynamics facility with HSL skirt. Skirt material is polyurethane coated nylon.

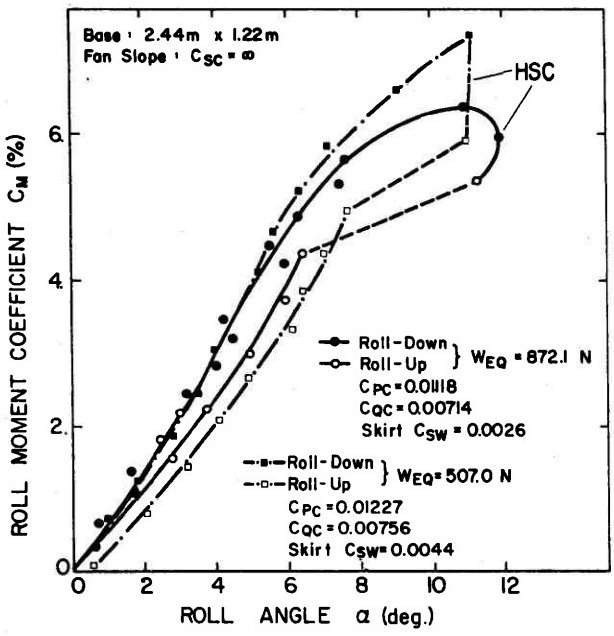
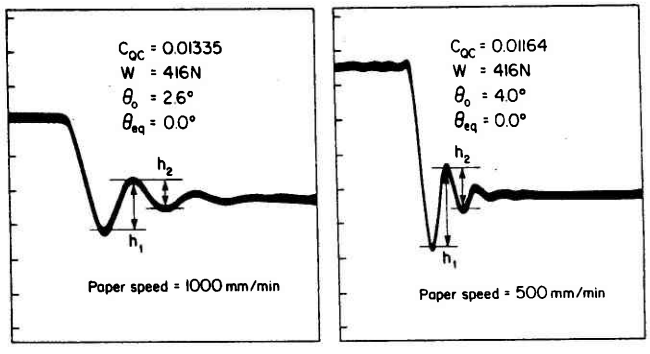


Fig. 9 Effect of gross model weight on the roll stiffness characteristic of the cushion dynamics facility with HSL skirt. Skirt material is polyurethane-coated nylon.

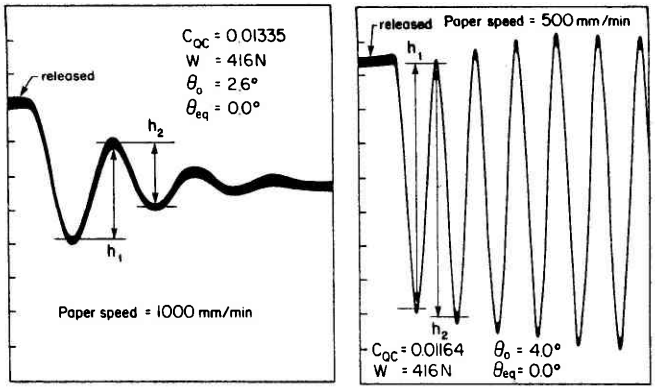
force between the skirt and ground results from cushion pressure acting on the inside of the segments. Similar hysteresis has also been measured in larger scale model tests on the UTIAS circular track vehicle.[5]

Static hysteresis becomes an important form of damping if it appears in the dynamics. Figures 10 and 11 give experimentally obtained dynamic pitch angle response traces of a 2.44m × 1.22m test facility equipped with the segmented skirt systems whose static pitch characteristics are given in Figs. 7 and 8. Note the increased damping in the case of the polyethylene skirt and that whereas the nylon-urethane skirt was exhibiting a limit cycle behaviour for the combined pitch-



(a) (b)

Fig. 10 Tracing of RVDT output giving pitch response to disturbance of the cushion dynamics facility with polyethylene skirt. (a) θ_o=2.6°, (b) θ_o=4.0°.



(a) (b)

Fig. 11 Tracing of RVDT output giving pitch response to disturbance of the cushion dynamics facility with nylon-urethane skirt. (a) θ_o=2.6°, (b) θ_o=4.0°.

heave motion, the resulting oscillation for the polyethylene skirt remained well damped. Similar behaviour has also been found at larger scale on the circular track vehicle with the segmented skirt system installed. Here, roll motion was induced as a result of gyroscopic coupling from the fan system and a combined pitch-heave-roll limit cycle type oscillation was obtained under certain conditions when the same lightweight nylon-urethane material was used for skirt construction. In Ref. 5 curves were presented which showed that the hysteresis measured in roll for a heavier skirt material used on the UTIAS circular track vehicle produced significant damping.

The traces given in Figs. 10 and 11 are also subject to flexibility effects which are discussed in detail for a conical skirt geometry in Ref. 6. Here it was shown that, in the absence of air escape area modulation with cushion pressure, increasing flexibility modulated the pneumatic capacitance and tended to make the system more unstable in heave. Stiffness measurements on the two materials showed that the nylon-urethane material was stiffer in the warp direction but less stiff in the fill direction than the polyethylene, which was isotropic. The combined effect of this on the cushion capacitance relative to the polyethylene has not been determined owing to the complex geometry of the segments and the material. It is expected that there is some increase in capacitance which plays a role in determining the onset of the limit cycle behaviour but that the improved damping with the polyethylene is mainly a result of the increased static hysteresis.

FULL SCALE HYSTERESIS - ACIB MEASUREMENTS

The measurements were made on February 25, 1983 at the Canadian Coast Guard terminal in Thunder Bay, Ontario. Only pure heave measurements were made. The vehicle operating point was altered by varying fan engine speed in small steps. After each speed change the vertical position and cushion pressure were allowed to stabilize. The vertical position was then measured using a surveyor's level which sited on three 1.3m graduated rods mounted on the deck as shown in Fig. 12. The corresponding cushion pressure was measured in two ways, once using a water manometer and once using a pressure gauge, both of which were mounted in the control room. The height of the geometric centre of the deck was found by fitting a plane through the vertical positions of the three measurement stations. The test results are given in Fig. 13.

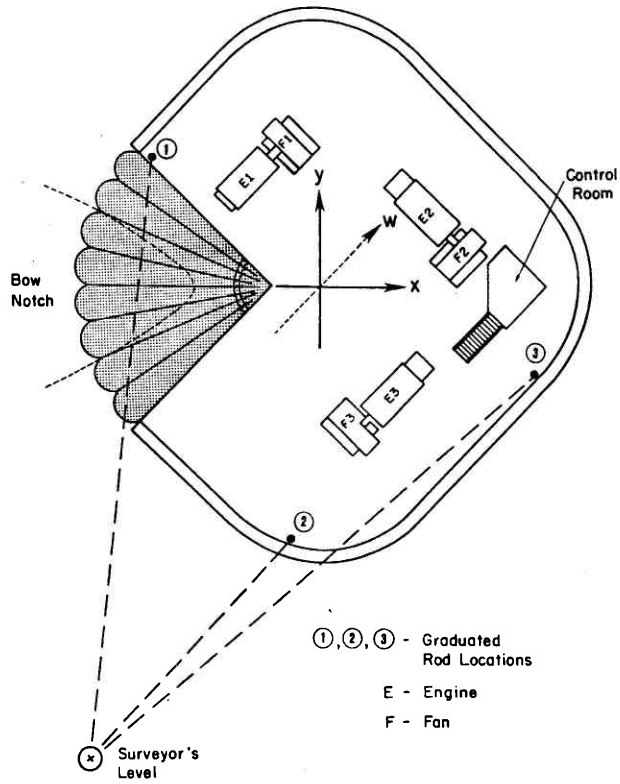


Fig. 12 ACIB layout showing location of graduated rods and surveyor's level.

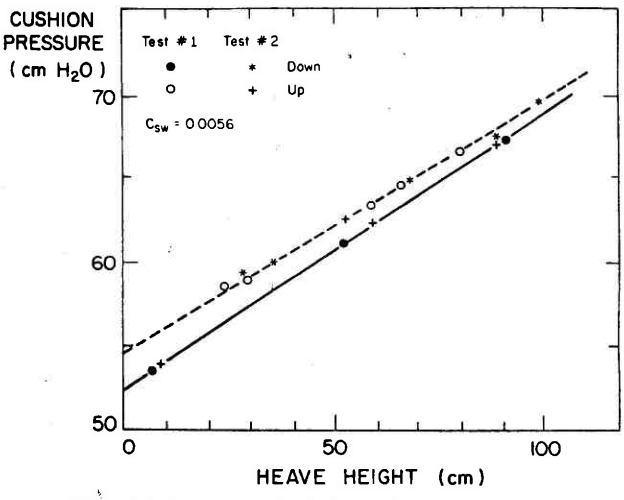


Fig. 13 Experimental data from heave cycle tests on ACIB.

Data from two down-up cycles are plotted in this figure. As can be seen, there is very little scatter. Also, the pressure versus height data are very linear, both downgoing and upgoing. The data show that the skirt supports about 4% of the gross weight when the vehicle hard structure is almost in contact with the ground. It supports about 1% during normal operation.

For segmented skirt systems, the roll stiffness, due to the geometrical shift in the centroid of the pressurized support area, is typically about 1-1.5% per degree roll. An estimate of the hysteresis one would expect in roll* due to skirt loads can be obtained from the heave data by using it to calculate typical skirt loads per unit perimeter. For example, when the pure heave skirt load is taken to be 2% the roll hysteresis can be roughly estimated as follows. Assume that the vehicle rotates about a centre of mass located at the geometric centre of the craft and that the hysteresis mechanism operates only during downgoing motion. The hysteresis moment contributed by the edges of the craft is then $\cong (b/2)\times(0.02/4)W$ where b is the beam and W the craft weight. For the other sides of the craft the moment arm varies from 0 to b/2 so the average moment contribution is $\cong (2/3)\times(b/2)\times(0.02/4)W$. The total roll moment hysteresis is then $\cong$ 0.42% of Wb. This method gives a conservative estimate of the hysteresis as any contribution due to the rising side is neglected. This amount of roll hysteresis is shown schematically in Fig. 14.

As noted earlier, roll and pitch hysteresis measured in models with a segmented skirt system

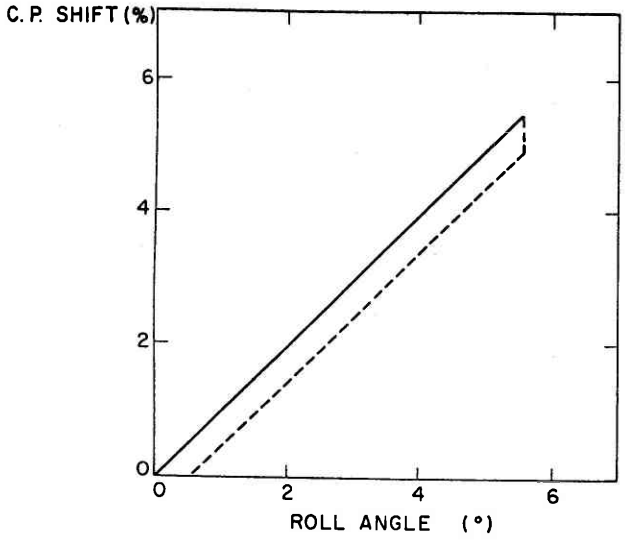


Fig. 14 Prediction of roll hysteresis from heave hysteresis measurements. Stiffness set nominally at 1% per degree for illustration purposes.

*Roll is meant to mean rotation about axis w in Fig. 12.

ranges from near zero to about 3% so that this conservative estimate places full scale hysteresis at the lower end of the order but is still significant. Also the amount of hysteresis measured in heave, 1-4%, is of the same order as load carried in the skirt material by a multicell cushion at various non-zero roll angles, $\cong$ 5%.

An estimate of the heave damping associated with hysteresis can be obtained by noting that the work done by hysteresis during an oscillation cycle must show up as a change in the kinetic energy of the air supported mass. This gives

Work Done = Change in Kinetic Energy

If the change in amplitude is small relative to the amplitude itself, this balance reduces to

$$2h_o F_s = Mh_o \Delta h \omega^2$$

where F_S is the skirt force, M is the air supported mass, h_o is the oscillation amplitude, Δh is the change in amplitude over one cycle, and ω is the oscillation frequency. Solving for Δh gives

$$\Delta h = \frac{F_s}{M} \frac{2}{\omega^2}$$

This shows that the change in amplitude over one cycle is independent of the amplitude. For F_S = 2% Mg and $\omega = 2\pi$ rad/sec, one obtains Δh = 1 cm.

CONCLUSIONS

The measurements of hysteresis in the heave characteristic of the ACIB have shown that model and full scale hysteresis are of the same order. In addition, other information[7,8] recently made available has shown that similar roll hysteresis is present in the BHC bag and finger design skirt system and a new Canadian hybrid design currently being tested.

The importance of this hysteresis is indicated in some recent work done at UTIAS on the dynamics of large air cushion platforms.[9] This work has shown that these cushions typically operate with very low phase margin or damping. Even well into the stable pressure-flow operating region, disturbance generated motions are only lightly damped. It is possible that, if properly exploited, skirt hysteresis could improve this situation.

The existence of hysteresis at full scale and its role in producing damping forces coupled with the lack of explanation of the physical mechanisms involved points out the need for in depth study of the phenomenon. A complete exploitation of the hysteresis and scaling of materials between model and full scale can only be achieved when the mechanisms are understood. Hysteresis, however, is only one of several factors to be considered when scaling skirt systems for dynamic experiments.[3] Depending on the system, skirt thickness, weight per unit area, elastic constants

and/or viscoelastic constants must be scaled as well. This can be quite difficult as many contradictory constraints are introduced when dimensional analysis is performed in consideration of these factors. The importance of hysteresis at full scale thus adds another factor to an already difficult scaling problem.

NOMENCLATURE

List of Symbols

b	craft hard structure beam
C_{PC}	nondimensional cushion pressure = P_a/P_{atm}
C_{QC}	nondimensional cushion flow
C_{SC}	fan slope coefficient
C_{ST}	skirt thickness coefficient = t_s/b
C_{SW}	skirt weight coefficient = W_s/P_c
F_s	skirt structural forces
h_o	heave cycle amplitude
M	vehicle mass
P_{atm}	atmospheric pressure
P_c	cushion pressure (gauge)
t_s	skirt thickness
W	vehicle weight
W_s	skirt weight per unit area
θ	pitch angle
ω	oscillation frequency

Abbreviations

ACIB	Air Cushion Ice-Breaker
ACV	Air Cushion Vehicle
BHC	British Hovercraft Corporation
UTIAS	University of Toronto, Institute for Aerospace Studies

ACKNOWLEDGEMENTS

This work was performed as part of a contract awarded by the Government of Canada's Transportation Development Centre (TDC). The support of Mr. J. E. Laframboise, Senior Project Officer for TDC, in scheduling the operation and arranging for this opportunity is sincerely appreciated. Special thanks also to Mr. Craig Carter of German-Milne and Mr. Jack Tarzwell of the Canadian Coast Guard whose on-site assistance was critical to the success of the testing.

REFERENCES

1. Sullivan, P. A., Hinchey, M. J., and Delaney, R. G., 'Static Roll Stiffness Characteristics of Two Multicell Type Air Cushion Systems', Journal of Terramechanics, Vol. 15, No. 1, 1978, pp. 15-41.

2. Sullivan, P. A., Hinchey, M. J., Hartmann, P. V., and Dupuis, A., 'Research Into Air Cushion Stability: 1978 Report', Transportation Development Centre, Transport Canada, TP-1760, TDC File No. D-500-431-1, January 1981.

3. Sullivan, P. A., Hinchey, M. J., Hartmann, P. V., Dupuis, A., Green, G., and Graham, T., 'Research into Air Cushion Stability: 1979 Report', Transportation Development Centre, Transport Canada, TP-3109-E, TDC File No. D-500-431-1, January 1982.

4. Sullivan, P. A., Hinchey, M. J., and Delaney, R. G., 'An Investigation of the Roll Stiffness Characteristics of Three Flexible Skirted Cushion Systems', UTIAS Report No. 213, March 1977.

5. Sullivan, P. A., Hartmann, P. V., and Graham, T. A., 'Application of System Identification Flight Analysis Techniques to the Pitch-Heave Dynamics of an Air Cushion Vehicle', Preprints from 16th Canadian Symposium on Air Cushion Technology, October 1982.

6. Graham, T. A., Sullivan, P. A., and Hinchey, M. J., 'Material Effects on the Dynamic Stability of a Flexible Skirted Air Cushion', AIAA 21st Aerospace Sciences Meeting, January 1983, Paper No. AIAA 83-0369.

7. ——— 'Stability and Control of Hovercraft: Notes for Commanders', United Kingdom Department of Industry Ship and Marine Technology Requirements Board BHC SP 4432, 1980.

8. Jones, D., Private Communication, 1983.

9. Hinchey, M. J., Sullivan, P. A., and Dupuis, A., 'Wave Propagation Effects on the Heave Dynamics of Large Air Cushion Platforms', UTIAS Technical Note No. 234, August 1982. Submitted to the Journal of Sound and Vibration.